

## **12. DATA REPORT: NUMERICAL EVALUATION OF DIFFUSE SPECTRAL REFLECTANCE DATA AND CORRELATION WITH CORE PHOTOS, ODP SITE 1165, WILD DRIFT, COOPERATION SEA, ANTARCTICA<sup>1</sup>**

Michele Rebesco<sup>2</sup>

### **ABSTRACT**

Two main alternating facies were observed at Ocean Drilling Program (ODP) Site 1165, drilled in 3357 m water depth into the Wild Drift (Cooperation Sea, Antarctica): a dark gray, laminated, terrigenous one (interpreted as muddy contourites) and a greenish, homogeneous, biogenic and coarse fraction-bearing one (interpreted as hemipelagic deposits with ice rafted debris [IRD]). These two cyclically alternating facies reflect orbitally driven changes (Milankovitch periodicities) recorded in spectral reflectance, bulk density, and magnetic susceptibility data and opal content changes. Superimposed on these short-term variations, significant uphole changes in average sedimentation rates, total clay content, IRD amount, and mineral composition were interpreted to represent the long-term lower to upper Miocene transition from a temperate climate to a cold-climate glaciation. The analysis of the short-term variations (interpreted to reflect ice sheet expansions controlled by 41-k.y. insolation changes) requires a quite closely spaced sampled record like that provided by the archive multisensor track. Among those, cycles are best described by spectral reflectance data and, in particular, by a parameter calculated as the ratio of the reflectivity in the green color band and the average reflectivity (gray). In this data report a numerical evaluation of spectral reflectance data was performed and substantiated by correlation with core photos to provide an objec-

<sup>1</sup>Rebesco, M., 2003. Data report: Numerical evaluation of diffuse spectral reflectance data and correlation with core photos, ODP Site 1165, Wild Drift, Cooperation Sea, Antarctica. In Cooper, A.K., O'Brien, P.E., and Richter, C. (Eds.), *Proc. ODP, Sci. Results*, 188, 1–27 [Online]. Available from World Wide Web: <[http://www-odp.tamu.edu/publications/188\\_SR/VOLUME/CHAPTERS/006.PDF](http://www-odp.tamu.edu/publications/188_SR/VOLUME/CHAPTERS/006.PDF)>. [Cited YYYY-MM-DD]

<sup>2</sup>Istituto Nazionale di Oceanografia e di Geofisica Sperimentale (OGS), Dipartimento Geofisica della Litosfera, Borgo Grotta Gigante 42/C, 34010 Sgonico (TS), Italy.  
[mrebesco@ogs.trieste.it](mailto:mrebesco@ogs.trieste.it)

tive description of the color variations within Site 1165 sediments. The resulting color description provides a reference to categorize the available samples in terms of facies and, hence, a framework for further analyses. Moreover, a link between visually described features and numerical series suitable for spectral analyses is provided.

## **INTRODUCTION**

Ocean Drilling Program (ODP) Site 1165 is situated in a water depth of 3357 m on the continental rise offshore from Prydz Bay and is drilled into mixed pelagic and hemipelagic sediments of the central Wild Drift (Shipboard Scientific Party, 2001b). The drift is an elongate sediment body formed by the interaction of sediment supplied from the shelf and westward-flowing currents on the continental rise. The site was selected to provide a record of sedimentation that extends back to the onset of contour current-influenced deposition. The drilling yielded a relatively continuous 999-m-thick sedimentary section of early Miocene to Pleistocene age deposits with only few minor (<2 m.y.) disconformities. Recovery was 86.4% in the advanced piston corer (APC) part of Hole 1165B (down to 147.9 meters below seafloor [mbsf]) and 57.3% in the extended core barrel (XCB) part (to 682.2 mbsf). After a single core was taken in a missing interval (~60 mbsf), continuous rotary core barrel (RCB) coring began at 673 mbsf in Hole 1165C with 80% recovery.

Sediments showed two cyclically alternating facies (Shipboard Scientific Party, 2000a): (1) dark gray laminated and homogeneous terrigenous clays (interpreted as muddy contourites) and (2) homogeneous biogenic-bearing greenish clays with a coarse sand to gravel-sized fraction (interpreted as hemipelagic deposits with ice rafted debris [IRD]). Such cyclical decimeter- to meter-scale alternations were reflected in the shipboard recorded reflectance (lightness), bulk density, and magnetic susceptibility. Spectral analyses in the depth domain for intervals with good magnetostratigraphic age control (upper Miocene/lower Pliocene) revealed the presence of Milankovitch periodicities, hence indicating that the physical property variations reflect orbitally driven changes in the marine depositional environment (Shipboard Scientific Party, 2000b). For brevity hereafter, these two facies will be referred to as “green” (instead of greenish gray facies) and “gray” (instead of gray to dark gray facies).

## **OBJECTIVES**

The main objective of drilling at Site 1165 was to obtain a proximal continental rise record of Antarctic glacial and interglacial periods for comparison with other sites. In fact, this site documents significant up-hole changes in average sedimentation rates, total clay content, IRD abundance, and mineral composition that were interpreted to represent the long-term lower to upper Miocene transition from a temperate climate to a cold-climate glaciation. Superimposed on this trend are the short-term variations (Milankovitch periodicities) represented by the decimeter- to meter-scale cyclic alternations of the two facies (green and gray) identified onboard. The overall sampling plan was more than adequate to investigate the long-term transition through the 999-m-thick drilled sedimentary section; however, detailed sampling strategies to examine these short-term variations failed. One of the principal

causes of such inadequacy was the lack of absolute and commonly shared criteria to define the facies and their boundaries. In fact, the boundary between the two facies is frequently transitional and is mostly shown by the color variation, the detection of which is subject individual perception.

During the leg, variations of the lightness factor ( $L^*$ ) recorded by the spectrophotometer were initially used to characterize cyclicity (see the “Color Alternations in Cores” section in Shipboard Scientific Party, 2001b). Nevertheless, a further inspection of the spectral reflectance data (Grützner et al., 2000) revealed that the color cycles are best described by the ratio of the reflectivity in the green color band and the average reflectivity (gray). In a similar way, spectral reflectance data from other ODP legs have been used for mineral composition and lithologic studies (Mix et al., 1995; Balsam et al., 1997; Ortiz et al., 1999) and investigations of sedimentary processes through grain-size variations (Wolf-Welling et al., 2001).

The objective of this data report is to perform a numerical evaluation of spectral reflectance data substantiated by correlation with core photos to provide an objective description of the color variations at Site 1165. The resulting color description will provide a reference to categorize the available samples in terms of facies and a framework for further analyses.

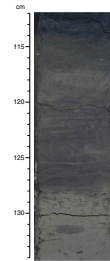
## LITHOLOGY

Site 1165 is divided into three lithostratigraphic units, the subdivision of which is mainly based on a combination of visual core description and biogenic and mineralogic composition:

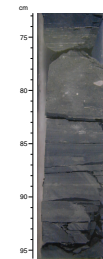
1. Unit I (0–63.8 mbsf; Pleistocene to early Pliocene age) consists of structureless brown clay and diatom-bearing clay, with one interval (Core 188-1165B-4H) characterized by alternations between two facies like those of Unit II.
2. Unit II (63.8–307.8 mbsf; middle to late Miocene age) is characterized by alternations of two main facies that differ in color and composition.
3. Unit III (307.8–999.1 mbsf; early Miocene age) comprises a section of thinly bedded planar-laminated claystone that is divided, like Unit II, into two main facies that differ in color, composition, and bedding characteristics.

Therefore throughout the hole, from early to at least late Miocene time, there is a regular repetition of two basic facies (Figs. F1, F2): (1) “green” (greenish gray bioturbated diatom-bearing mud with foraminifers and dispersed clasts and lonestones) and (2) “gray” (dark gray almost barren laminated mud) (Rebesco et al., 2001). In general (Fig. F3), the green facies is almost devoid of primary structures, whereas the gray one contains silt lamina (in the lower part of the hole), color (light/dark) banding (in the upper part of the hole), and a number of lightening-upward intervals (without any evident grain-size variation). Bioturbation, predominantly consisting of horizontal burrows, is more rarely observed in the lower part of the gray facies and becomes progressively visible toward its upper boundary. Also as a consequence of such distribution of the bioturbation process, the lower boundary of the gray facies is mostly sharp, whereas its upper boundary is generally transitional to the

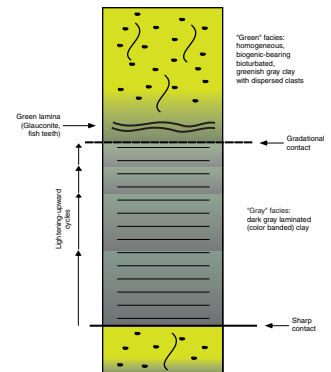
**F1.** Contact between green and gray facies, p. 11.



**F2.** Contact between gray and green facies, p. 12.



**F3.** Model of the green and gray facies, p. 13.



green one. In fact, local downward burrowing that introduced lighter (more greenish) sediments into the darker underlying beds is partly responsible for the transitional character of the lower boundary of the green facies. Such trace fossils that introduce material from a facies of one color into the underlying facies of another color indicate that color cycles in these sediments are primarily a depositional feature rather than the result of diagenesis (Boyd et al., 1994). General upward variation trends in the sedimentary section of Site 1165 include overall increasing occurrence of IRD, biogenic content, and bioturbation and decreasing average sedimentation rate and silt lamina occurrence. The alternation of the two facies and the variation in their relative thickness result in a complex rhythmic sedimentation with cycles at different scales (ranging from centimeters to tens of meters) nested together (Fig. F4). This rhythmic sedimentation changes in character throughout the 999-m sedimentary section and is locally difficult to recognize. Though the cores are highly fractured in the deeper part of the section, the most evident cycles are still recorded by the spectral reflectance data (Fig. F5). The gray facies was interpreted as contouritic sediment deposited during maximum ice advances, whereas the green facies was inferred to indicate hemipelagic deposition under warmer climate conditions.

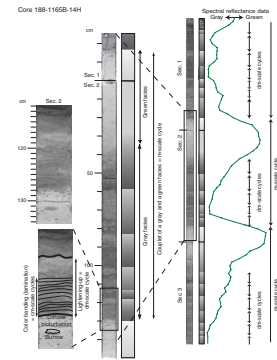
## SPECTRAL AND COMPOSITIONAL ANALYSES

Spectral analyses on depth and time series of diffuse spectral reflectance, multisensor core logs, and X-ray fluorescence (XRF) scan data from Cores 188-1165B-8H through 15H (~5–9 Ma) demonstrate that variance is dominated by orbital frequencies, as predicted by the Milankovitch theory (Grützner et al., 2000). The detected obliquity and precession cycles were in turn used to improve the shipboard sedimentation rates. Refined sedimentation rates together with opal measurements allowed quantification of changes in the fluxes of biogenic opal and terrigenous material at a high resolution (Grützner et al., 2001b). Opal measurements on selected samples indicated a range of 5% to 30% for the biogenic component (Grützner et al., 2001a). A multiple linear regression approach combining discrete opal data and continuous core logging records was used to estimate percent biogenic silica at a high resolution. Maximum silica values are typical for green facies, indicating hemipelagic sedimentation under warmer climate conditions. Compared to opal-rich layers, terrigenous-dominated intervals display much lower green/gray color ratios and are characterized by higher densities, magnetic susceptibilities, and iron contents. The terrigenous-dominated gray facies are interpreted to have been deposited during ice sheet expansions controlled by variations in solar insolation dominated by 41-k.y. (obliquity) cycles (Grützner et al., in press).

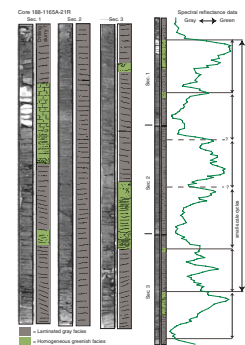
## METHODS

Reflectance of visible light from the surface of the archive halves of cores from ODP Leg 188 was routinely measured downcore (Shipboard Scientific Party, 2001a) using a Minolta spectrophotometer (model CM-2002) mounted on the archive multisensor track (AMST). The purpose was to provide a continuous stratigraphic record of color variations downcore for visible wavelengths (VIS; 400–700 nm). The measurements were automatically recorded by the AMST and logged into the

F4. Complex rhythmic sedimentation, p. 14.



F5. Rhythmic sedimentation, p. 15.



shipboard Oracle database (Janus). Each measurement consists of 31 separate determinations of reflectance in 10-nm-wide spectral bands from 400 to 700 nm. Additional detailed information about measurement and interpretation of spectral reflectance data with the Minolta spectrophotometer can be found in Balsam et al. (1997, 1998, 1999) and Balsam and Damuth (2000).

The numerical evaluation of spectral reflectance data from site 1165 included a number of successive steps:

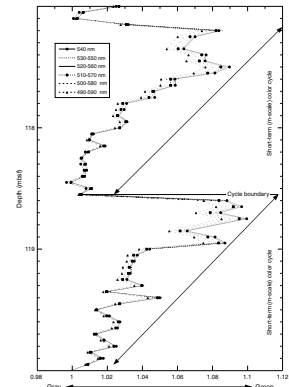
1. Downloading of the data. Data from Holes 1165B and 1165C were downloaded from the Janus database (note that Cores 188-1165B-2H through 76X and 188-1165C-1R were sampled every 5 cm, whereas Core 188-1165B-1H and 188-1165C-2R through 35R were sampled every 2 cm).
2. Compilation. A single record was obtained from arranging the data from the two holes (note that Hole 1165C was washed down to a depth of 54 mbsf, where a single core was taken at an interval that had been missed in Hole 1165B).
3. Manual editing of the record. Samples that laid outside a pre-established error band surrounding the reference curve (computed by a moving average for comparison against the data) were compared with the core photo and removed if an anomaly was encountered. Moreover, overlapping samples (same depth) were removed. Anomalies encountered in the data were the following: presence of stones or mud clasts, holes, fractures, voids, or samples taken too close to the edge of the section. The list of the removed samples and pertinent motivations is shown in Table T1.
4. Sensitivity tests to define the parameter, derived from the raw data, that best describes the color cycles. Such analysis is based on the assumption that the significant parameter is a ratio between the average reflectivity in the green color bands (that should describe the green facies) and the average reflectivity of all bands (that should describe the gray facies). Considering that the green band is generally contained between 490 and 600 nm (with some variability depending on one's visual perception) and after having verified against the record (within evident cycles in Core 188-1165B-14H) that the most sensitive band is 540 nm, two kinds of tests were performed:

- a. To define the number of bands to be considered and
- b. To define which bands are to be considered.

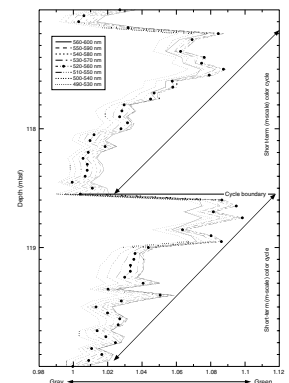
In both tests a ratio between the average reflectivity of certain color bands (green) and the average reflectivity of all bands (gray) is computed for the data between 117 and 120 mbsf (Core 188-1165B-14H). Test a shows six different curves obtained with a growing number of bands considered in the numerator (green), from the 540-nm band alone, to eleven bands (490–590 nm). This test (Fig. F6) shows that the number of bands is not a critical factor since the six curves are quite similar (partly overlapping) and show the same cyclicity. In test b, eight different curves were obtained with a moving selection of five bands considered in the numerator (green), from the 490- to 530-nm frequency band and the last with the 560- to 600-nm bands). This test (Fig. F7) shows that, within the 490- to 600-nm frequency band, the band selection is not a crit-

T1. Samples removed, p. 22.

F6. Definition of number of bands to consider, p. 16.



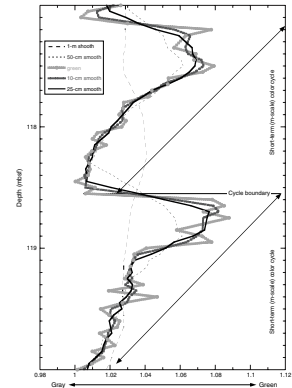
F7. Definition of which bands to consider, p. 17.



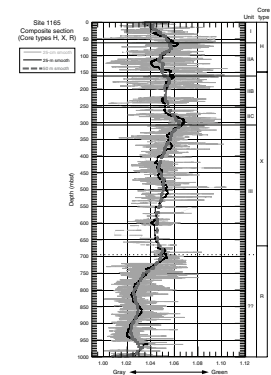
ical factor, though more sensitive than the number of bands. In fact, the same cyclicity is shown by the eight curves, which are partly overlapping and gathered around the curve produced with the 520- to 560-nm frequency band. Considering the results of the two tests, it was decided to consider in the numerator (green) a high number of bands centered on the 540-nm band. Ten bands ranging from 500 to 590 nm inclusive were hence considered for the calculation of the “green parameter” (ratio between average green reflectivity and average gray reflectivity).

5. Smoothing of the curve. To analyze the meter-scale color cycles, the high-frequency variations (centimeter to decimeter scale) were “filtered,” computing a moving average of the curve. Test c (Fig. F8) was made to calibrate the length of the windows of the moving average by comparing five curves produced using windows of different lengths ranging from 5 cm (no smoothing) to 1 m. The 25-cm window is the one that appears to work best, since the meter-scale cycles are completely leveled off by the 1-m average and still poorly defined by the 50-cm average, whereas disturbing high-frequency variability is preserved by the 10- and 5-cm averages. Note that, as discussed by Melnyk et al. (1994), this averaging process leads to the loss of  $(N/2-1)$  data points at both ends of the curve (where  $N$  is the length of the moving average). This loss was remedied by progressively reducing down to 1 sample the window length at the beginning and at the end of the record, so no data points were lost.
6. Normalization of the 25-cm averaged “green parameter.” Since the meter-scale cyclicity is superimposed on larger-scale trends, it is necessary to remove the larger-scale variations. To calibrate the length of the window of the moving average to be used to produce the larger-scale curve, a comparative test was performed. In test d, two curves obtained with 25- and 50-m windows, respectively, are compared against the 25-cm averaged “green parameter.” This test (Fig. F9) shows that the 50-m smoothed curve is excessively diverging from the 25-cm curve and is too leveled to show some decameter-scale trends that will be discussed in this paper (e.g., between 105 and 135 mbsf and 280 and 320 mbsf). It was hence decided to normalize the 25-cm averaged “green parameter” against a 25-m averaged curve.
7. Plot of 50-m-long segments of the normalized curve with indication of the core and section breaks (Fig. F10A–F10N). A vertical line is shown in correspondence of the zero value as reference; samples with negative values correspond to gray facies, whereas positive values correspond to green facies. Note that the thin seventh sections eventually present in cores were not indicated because they are not discernible at this scale. Only cores in Hole 1165B (cores from APC [type H] and XCB [type X]) were plotted so far because adequate data analysis of the deep part (RCB section) of Site 1165 will require additional care, due to highly fractured lithology, differences in color and lightness with respect to the upper part, and very small thickness of the green facies (a few centimeters) (see Fig. F2).
8. Verification against the core photos. Such validation was performed using section by section visual matching of the plots of the normalized curve with the color core photos. The visual core description sheets and the graphic logs compiled onboard were also considered. The facies interpretation derived from visual de-

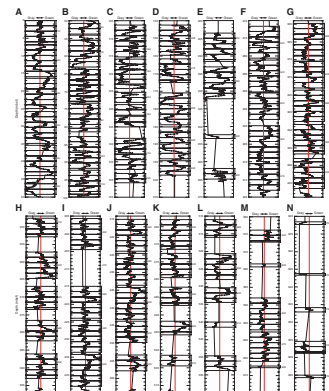
F8. Calibration of the window length for curve smoothing, p. 18.



F9. Calibration of the window for normalizing the green parameter, p. 19.



F10. Plots of segments of normalized green parameter, p. 20.



scription (photo, and onboard sheets) is adequately matched by the proposed normalized curve (Fig. F11), hence providing a link between descriptive features and numerical series suitable for spectral analyses. Spectral reflectance data from Site 1165 are provided in Table T2.

## RESULTS

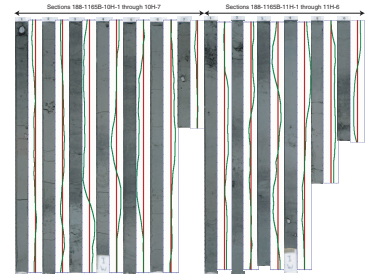
### Description of the Meter-Scale and Larger Trends

The alternating green–gray facies is not evident in the uppermost lithostratigraphic unit (Unit I) dating back to the Pliocene–Pleistocene (above 63.8 mbsf). Within this unit, which is characterized by a yellowish to brown color, the calculated parameter is not appropriate, though it shows some variations, especially in Core 188-1165B-4H, which is characterized by alternations between two facies similar to those of Unit II (Fig. F10A).

The facies alternation begins at the top of Unit II (within Core 188-1165B-8H) where each facies ranges from ~50 cm to 2 m in thickness (Fig. F10B). The cycles (each constituted by a green–gray couplet) in the uppermost part of Subunit IIA are relatively symmetrical, with the thickness of the two facies generally comparable (~50 cm each) and with similar transitional boundaries. An exception is represented by the cycle in the upper part of Core 188-1165B-9H, showing a relatively thick green facies with a sharp upper boundary. The well-developed cyclicity observed during the leg is definitively present in Core 188-1165B-10H and below, where the typical 1.5-m-thick cycles with transitional gray to green boundaries and sharp green to gray boundaries are visible at their best between 87 and 90 mbsf (Fig. F10B). Such cycles are quite similar in shape to the typical cycles shown in Core 188-1165B-14H (Fig. F4), though the gray facies is generally thicker in the interval between 110 and 140 mbsf (Figs. F9, F10C). Subunit IIB generally shows thicker cycles, with each facies ~2–3 m thick (Fig. F10D, F10E). Most of Subunit IIC, and Cores 188-1165B-34X through 36X in particular, shows very thick (>3 m) green facies (Fig. F10F, F10G). Therefore, although the green and gray facies are alternating at the meter scale throughout the whole Unit II, the ratio between the thickness of the two facies is changing. The changes in such thickness ratio constitute a larger (decameter) scale trend (Fig. F9). Such a trend does not show any evident cyclical behavior.

As core preservation and recovery percentage decrease downward, the facies alternation is likewise progressively less clear downward within Unit III. In these progressively more fractured cores, bedding characteristics help to identify the two facies, the gray one being more fissile and fractured than the relatively ductile green one. The upper 100 m of Unit III shows a vague facies alternation on a several-meter-thick base. In fact, see, for example, Core 188-1165B-42X, which is almost entirely green, and the underlying Core 188-1165B-43X, which is almost entirely gray (Fig. F10H). A cyclicity produced by a major 1.5-m-thick green facies every ~15 m becomes progressively evident in the underlying 100 m (e.g., the green facies in Sections 188-1165B-48X-3 and 50X-1 surrounded by a predominantly gray interval) (Fig. F10I, F10J). Between 450 and 700 mbsf the facies alternation is still visible, though not evident, when both color and bedding characteristics are employed as identifying criteria. Nevertheless, no rhythmicity is recognizable in

F11. Example of match between cores with normalized green parameter, p. 21.



T2. Spectral reflectance data, Site 1165, p. 24.

this part of the sedimentary section, possibly also as a consequence of the poor recovery (Fig. [F10K](#), [F10L](#), [F10M](#), [F10N](#)). Depending on core conditions and recovery, good examples of green facies with excellent burrowing episodes were identified also in the very deep part of the drilled section (e.g., in Cores 188-1165B-58X, 59X, and 60X) (Fig. [F10L](#)).

## **ACKNOWLEDGMENTS**

This research used data provided by the Ocean Drilling Program (ODP). ODP is sponsored by the U.S. National Science Foundation (NSF) and participating countries under management of Joint Oceanographic Institutions (JOI), Inc. Funding for this research was provided by the Italian Programma Nazionale di Ricerche in Antartide (PNRA) through the projects SEDiment Drifts of the ANtartic Offshore (SEDANO) and ODP Leg 178. Jens Grützner is sincerely thanked for having provided essential information on the spectral and compositional analyses. Carl Richter and an anonymous reviewer are acknowledged for their helpful comments and accurate suggestions, which improved this manuscript.

## REFERENCES

- Balsam, W.L., and Damuth, J.E., 2000. Further investigations of shipboard vs. shore-based spectral data: implications for interpreting Leg 164 sediment composition. *In* Paull, C.K., Matsumoto, R., Wallace, P., and Dillon, W.P. (Eds.), *Proc. ODP, Sci. Results*, 164: College Station, TX (Ocean Drilling Program), 313–324.
- Balsam, W.L., Damuth, J.E., and Schneider, R.R., 1997. Comparison of shipboard vs. shore-based spectral data from Amazon-Fan Cores: implications for interpreting sediment composition. *In* Flood, R.D., Piper, D.J.W., Klaus, A., and Peterson, L.C. (Eds.), *Proc. ODP, Sci. Results*, 155: College Station, TX (Ocean Drilling Program), 193–215.
- Balsam, W.L., Deaton, B.C., and Damuth, J.E., 1998. The effects of water content on diffuse reflectance measurements of deep-sea core samples: an example from ODP Leg 164 sediments. *Mar. Geol.*, 149:177–189.
- , 1999. Evaluating optical lightness as a proxy for carbonate content in marine sediment cores. *Mar. Geol.*, 161:141–153.
- Boyd, R., Huang Z., and O'Connell, S., 1994. Milankovitch cyclicity in Late Cretaceous sediments from Exmouth Plateau off northwest Australia. *In* de Boer, P.L., and Smith, D.G. (Eds.), *Orbital Forcing and Cyclic Sequences*. Spec. Publ.—Int. Assoc. Sedimentol., 19:145–166.
- Grützner, J., Forsberg, C., and Rebesco, M., 2000. Orbitally controlled sedimentation at the east Antarctic continental rise: evidence from ODP Site 1165 (Leg 188, Prydz Bay). *Eos*, OS22A-05. (Suppl.)
- Grützner, J., Rebesco, M., Cooper, A.K., Forsberg, C.F., Kryc, K.A., and Wefer, G., in press. Evidence for orbitally controlled size variations of the East Antarctic Ice Sheet during the late Miocene. *Geology*.
- Grützner, J., Rebesco, M., Forsberg, C.F., and Cooper, A.K., 2001a. Evidence for palaeoclimatic variability at the East Antarctic continental rise (ODP Site 1165) inferred from spectral analysis of high-resolution core logging data. *In* Florindo, F., and Cooper, A.K. (Eds.), *Quaderni di Geofisica, Extended Abstracts for the International ANTOSTRAT Symposium on the Geologic Record of the Antarctic Ice Sheet from Drilling, Coring and Seismic Studies*: Rome (Istituto Nazionale di Geofisica e Vulcanologia), 16:81–82.
- Grützner, J., Rebesco, M., Forsberg, C.F., Cooper, A.K., and Wefer, G., 2001b. Cyclic sedimentation offshore east Antarctica during the late Miocene: results from ODP Site 1165, Prydz Bay. *In* *Abstracts of the CC02 Symposium (High Latitude Cenozoic–Quaternary Ice Sheets and Climate—Records of their Role in Global Climate Change)*. XI Eur. Union Geosci. Meet., 11:4. (Abstract)
- Melnyk, D.H., Smith, D.G., and Amiri-Garroussi, K., 1994. Filtering and frequency mapping as tools in subsurface cyclostratigraphy, with example from the Wessex Basin, UK. *In* de Boer, P.L., and Smith, D.G. (Eds.), *Orbital Forcing and Cyclic Sequences*. Spec. Publ.—Int. Assoc. Sedimentol., 19:35–46.
- Mix, A.C., Harris, S.E., and Janecek, T.R., 1995. Estimating lithology from noninvasive reflectance spectra: Leg 138. *In* Pisias, N.G., Mayer, L.A., Janecek, T.R., Palmer-Julson, A., and van Andel, T.H. (Eds.), *Proc. ODP, Sci. Results*, 138: College Station, TX (Ocean Drilling Program), 413–427.
- Ortiz, J., Mix, A.C., Harris, S., and O'Connell, S., 1999. Diffuse spectral reflectance as a proxy for percent carbonate content in North Atlantic sediments. *Paleoceanography*, 14:171–186.
- Rebesco, M., Grützner, J., Forsberg, C.F., and Cooper, A.K., 2001. Miocene rhythmic sedimentation in the Wild Drift, Antarctica (ODP Site 188-1165). *In* Florindo, F., and Cooper, A.K. (Eds.), *Quaderni di Geofisica, Extended Abstracts for the International ANTOSTRAT Symposium on the Geologic Record of the Antarctic Ice Sheet from Drilling, Coring and Seismic Studies*: Rome (Istituto Nazionale di Geofisica e Vulcanologia), 16:159–160.

- Shipboard Scientific Party [ODP Leg 188], 2000a. Lithostratigraphy of continental shelf, trough-mouth fan and sediment drift deposits, ODP Leg 188, Prydz Bay, East Antarctica. *Eos*, S273-274. (Suppl.)
- , 2000b. Physical property changes as a proxy for East Antarctic sedimentation: first results from ODP Leg 188 (Prydz Bay). *Eos*, S272. (Suppl.)
- , 2001a. Explanatory notes. In O'Brien, P.E., Cooper, A.K., Richter, C., et al., *Proc. ODP, Init. Repts.*, 188, 1–66 [CD-ROM]. Available from: Ocean Drilling Program, Texas A&M University, College Station TX 77845-9547, USA.
- , 2001b. Site 1165. In O'Brien, P.E., Cooper, A.K., Richter, C., et al., *Proc. ODP, Init. Repts.*, 188, 1–191 [CD-ROM]. Available from: Ocean Drilling Program, Texas A&M University, College Station TX 77845-9547, USA.
- Wolf-Welling, T.C.W., Cowan, E.A., Daniels, J., Eyles, N., Maldonado, A., and Pudsey, C.J., 2001. Data report: Diffuse spectral reflectance data from rise Sites 1095, 1096, and 1101 and Palmer Deep Sites 1098 and 1099 (Leg 178, western Antarctic Peninsula.) In Barker, P.F., Camerlenghi, A., Acton, G.D., and Ramsay, A.T.S. (Eds.), *Proc. ODP, Sci. Results*, 178 [Online]. Available from World Wide Web: <[http://www-odp.tamu.edu/publications/178\\_SR/chap\\_21/chap\\_21.htm](http://www-odp.tamu.edu/publications/178_SR/chap_21/chap_21.htm)> [Cited 2001-11-16].

**Figure F1.** Detailed color photo showing a contact between green and gray facies (Section 188-1165B-14H-2; ~119 mbsf). The green facies (below 128 cm from the top of the section) is homogeneous, with evident burrows and bioturbation throughout. Its upper contact is affected by bioturbation, though was likely sharp at the moment of deposition. Within the overlying gray facies a decimeter-scale lightening-upward cycle is visible between 128 and ~117 cm from the top of the section. In turn, within the lightening-upward cycle faint lamination and color banding is visible.

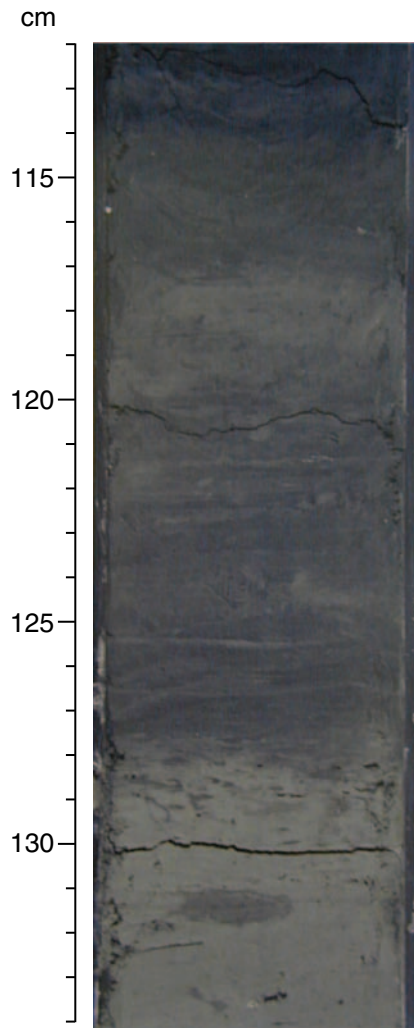


**Figure F2.** Detailed color photo showing a contact between gray and green facies (Section 188-1165C-21R-3; ~859 mbsf). The green facies (between ~83 and 77 cm from the top of the section) is homogeneous, with evident dispersed clasts (e.g., the angular light centimeter-sized spot at 79 cm) and large foraminifer bulbs (most of the visible white circular spots). The upward transition to the overlying gray facies is relatively sharp at ~77 cm (immediately underlying an evident fracture) as revealed by the evident change in the sedimentary structures (appearance of lamination with light-colored silty partings) and by a slight color change. Nevertheless, the main color boundary is at 74 cm, a few centimeters above the lithologic transition. Such a rarely observed shift between color and facies boundaries is likely related to upward postdepositional (diagenetic) chemical migration. Conversely, the downward transition to the underlying gray facies is quite gradational and is not completely achieved within the interval shown in photo. Within such a transition, intermediately greenish gray, darker laminations (e.g., 86 cm) and greener horizontal bioturbations (91.5 cm) are present. The lamination with silty partings typical of the gray facies of this deep part of the sedimentary succession is present below such transition (below 83 cm).

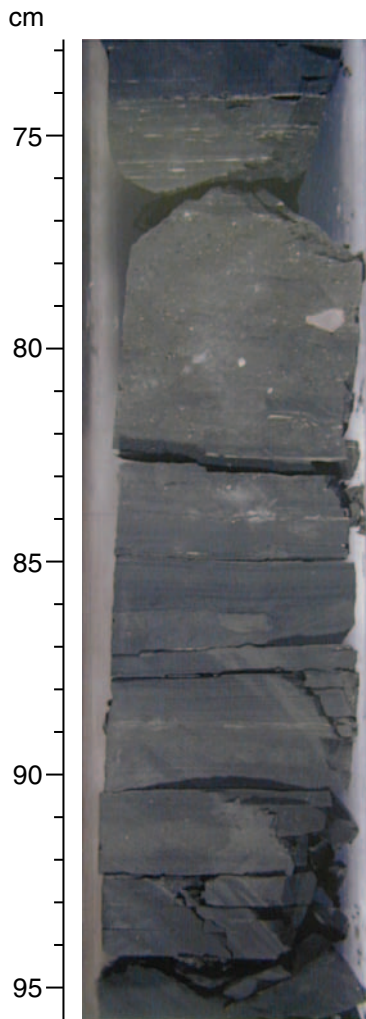


**Figure F3.** Simplified facies model of the green and gray facies identified at Site 1165. This schematic drawing is based on the most commonly observed trends during onboard visual core description between 100 and 200 mbsf. Similar green–gray couplets were observed throughout the sedimentary section down to 999 mbsf, though an overall decreasing occurrence of IRD, biogenic content, and bioturbation and increasing average sedimentation rate and silt lamina occurrence was observed.

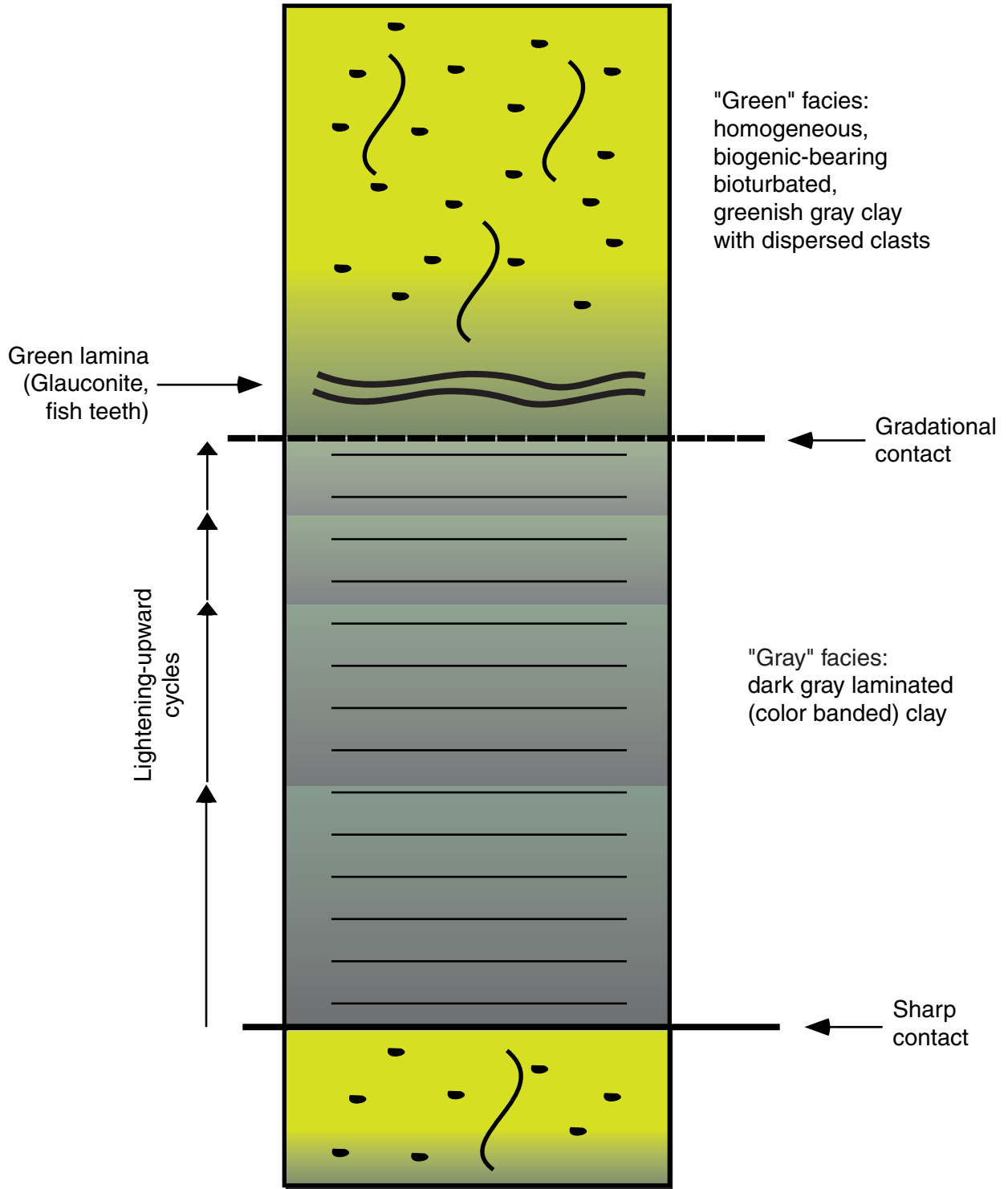


**Figure F4.** Composite diagram showing the complex rhythmic sedimentation with cycles at different (centimeter to meter) scales nested together within Core 188-1165B-14H (modified after Rebesco et al., 2001). The centimeter-scale cycles are revealed by color banding and lamination (see the interpreted black-and-white photo in the left bottom). Such cycles are included within decimeter-scale cycles characterized by lightening-upward intervals. In turn, these cycles are included within gray facies (see the black-and-white photo in the center and the synthetic interpretation on its right). Finally, meter-scale cycles are constituted by a couplet of gray and green facies. The decimeter- and meter-scale cycles are precisely recorded by diffuse spectral reflectance data (see the ratio of the reflectivity in the green color band vs. the average reflectivity on the right side of the diagram). Moreover, larger-scale (several decameters) cycles (not shown here) are produced by the variation in ratio between the thickness of the two facies.

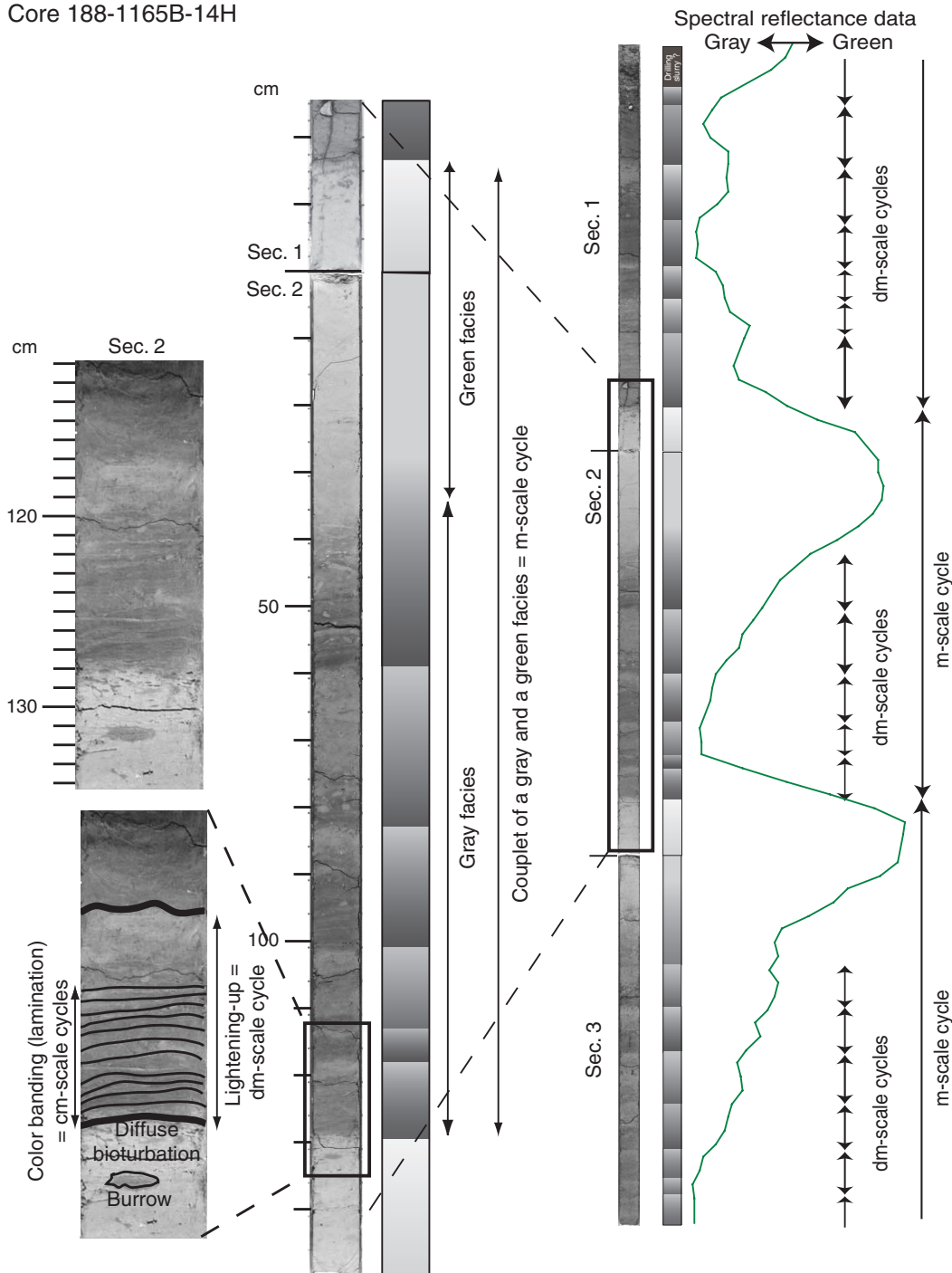


**Figure F5.** Composite diagram showing the rhythmic sedimentation within Core 188-1165C-21R. Because of the increased sediment darkness with depth, the difference in color between the green and gray facies at this depth (>850 mbsf) is less visible than in the upper part of the hole. Nevertheless (see the section photos and the pertinent onboard-drawn graphic logs on the left side of the figure), the green and gray facies may be distinguished on the basis of their sedimentary structure: the gray one is laminated (fractured), whereas the green one is bioturbated (lamination is hence less evident or completely obliterated). Notwithstanding the highly fractured condition of the core, several decimeter-scale cycles are recorded by spectral reflectance data (see the ratio of the reflectivity in the green color band vs. the average reflectivity on the right side of the diagram). However, since the sedimentation rate in this part of the hole is estimated to be about three times that within Core 188-1165B-14H, the equivalent of the 1.5-m-scale cycles observed uphole is likely represented here by the 4-m-thick cycle bounded by the thicker green facies, with the thinner greens corresponding to the smaller-scale cyclicity within the gray facies.

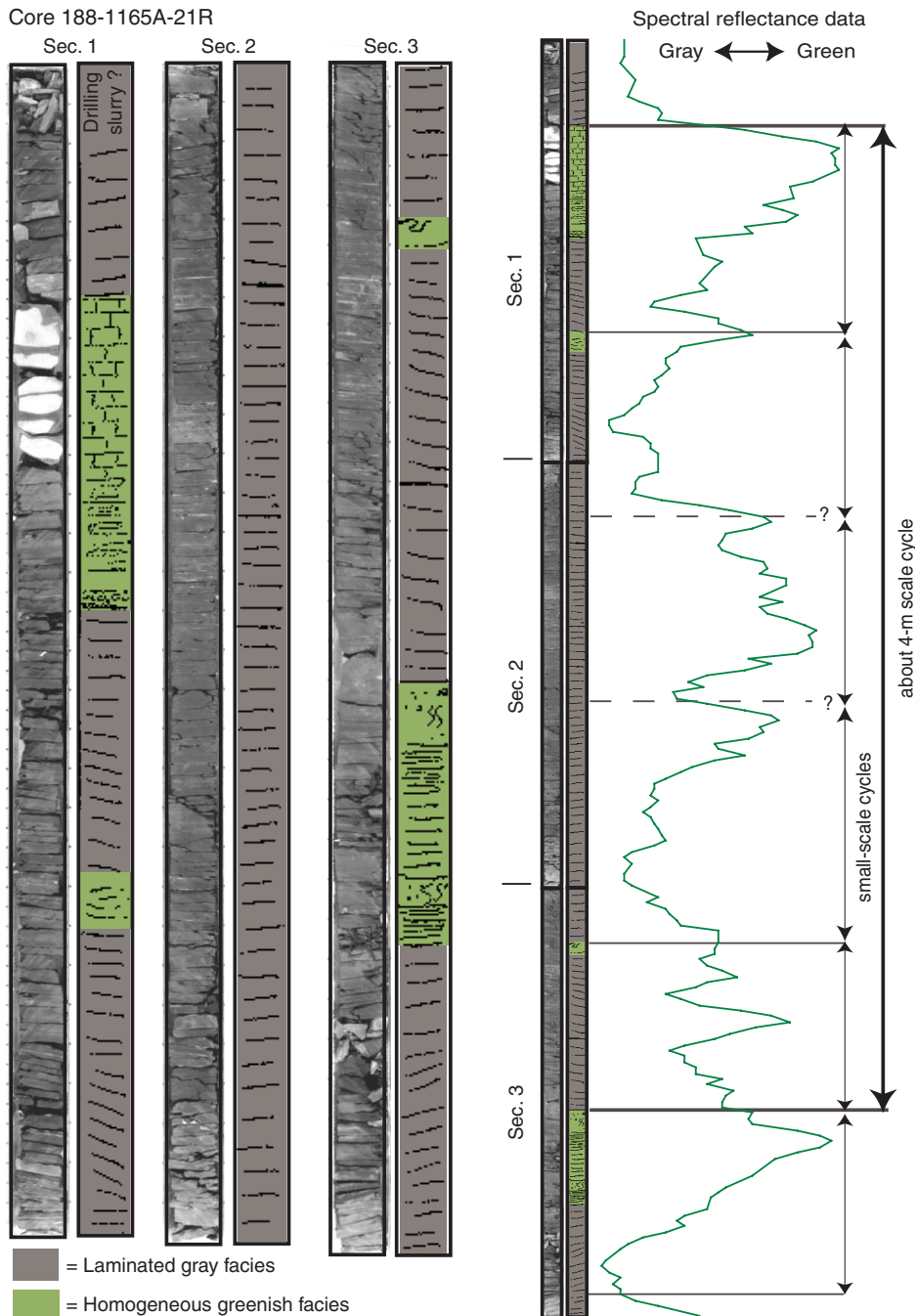


Figure F6. Plot of the sensitivity test to define the number of bands to be considered. The ratio between the average reflectivity of certain color bands (green) and the average reflectivity of all bands (gray) is computed for the data between 117 and 120 mbsf (Core 188-1165B-14H). Six different curves, obtained with a growing number of bands considered in the numerator (from the 540-nm band alone to 11 bands spanning from 490 to 590 nm), are shown. The six curves are quite similar (partly overlapping) and show the same cyclicity, indicating that the number of bands is not a critical factor.

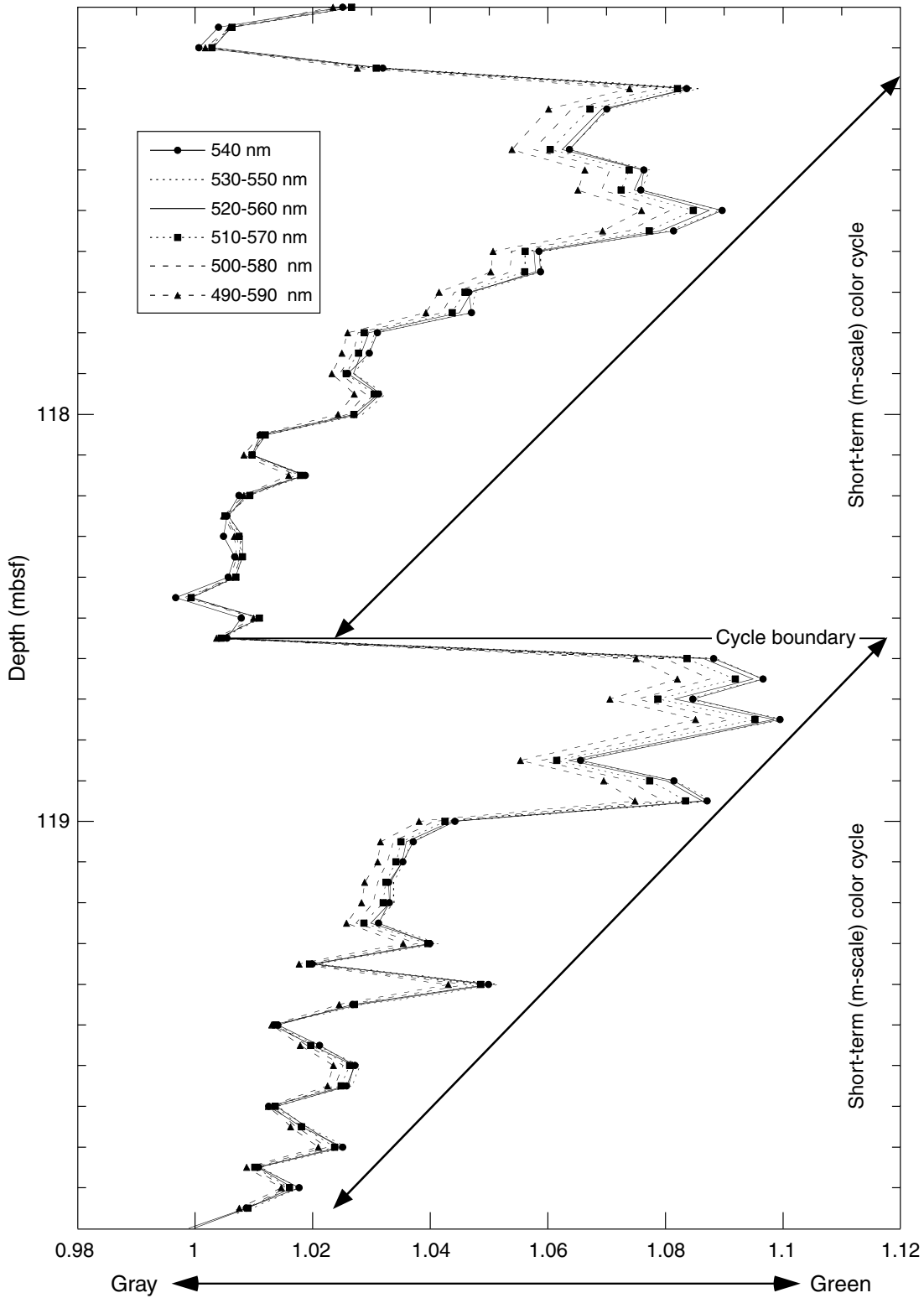


Figure F7. Plot of the sensitivity test to define which bands are to be considered. The ratio between the average reflectivity of certain color bands and the average reflectivity of all bands is computed for the data between 117 and 120 mbsf. Eight different curves obtained with a moving selection of five bands considered in the numerator (green), from 490 to 600 nm (the first curve being with the 490- to 530-nm frequency bands and the last with the 560- to 600-nm bands), are shown. The eight curves are partly overlapping and gathered around the curve produced with the 520- to 560-nm frequency band, indicating that the band selection is not a critical factor, though more sensitive than the number of bands.

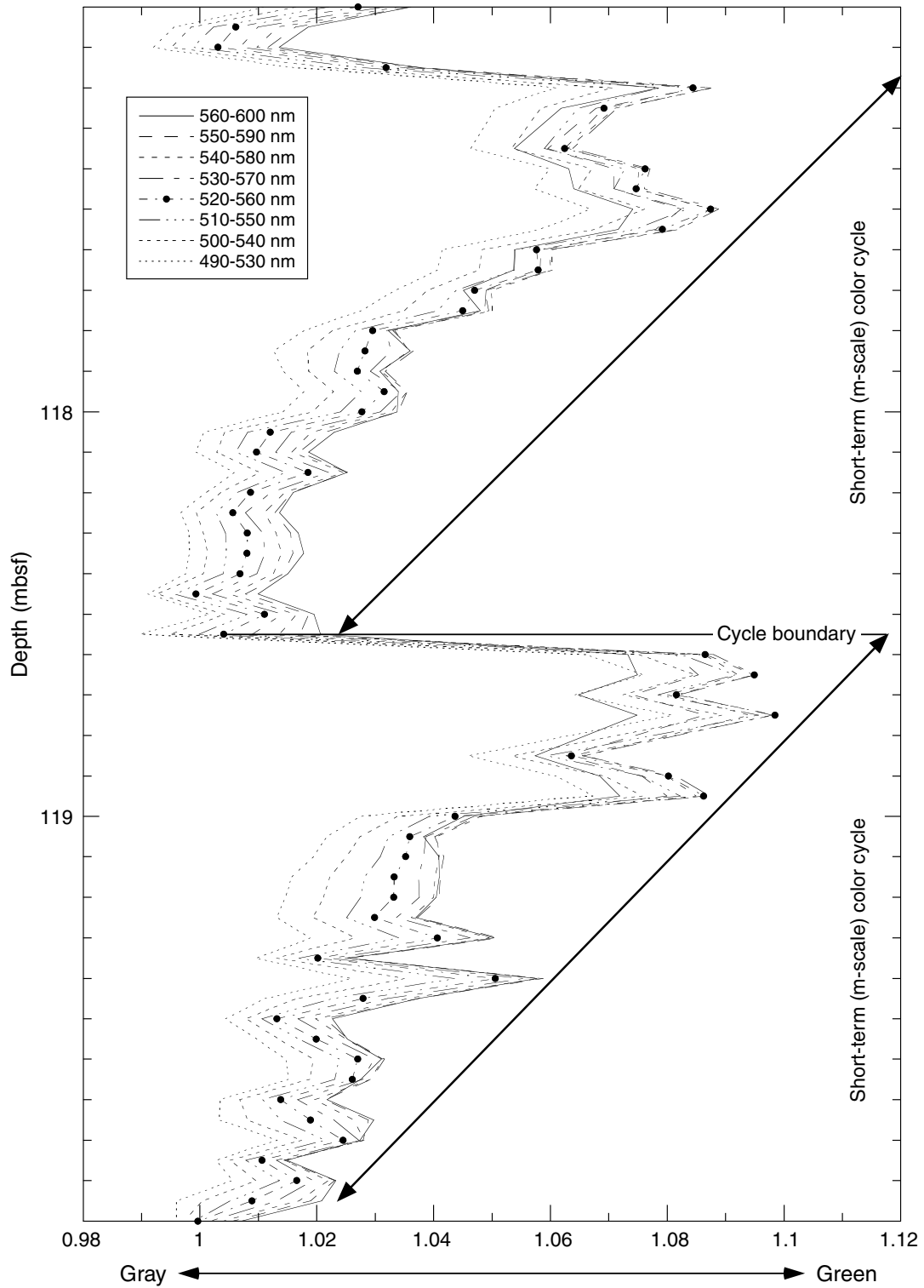


Figure F8. Plot of the comparative test to calibrate the length of the windows of the moving average for filtering the high-frequency variations (centimeter to decimeter scale) of the color. Five curves produced using windows of different lengths ranging from 5 cm (green; no smoothing) to 1 m are shown for the data between 117 and 120 mbsf. The 25-cm window is the one that appears to work best to describe the meter-scale color cycles, since these are completely leveled off by the 1-m and 50-cm averages, whereas disturbing high-frequency variability is preserved by the 10- and 5-cm averages.

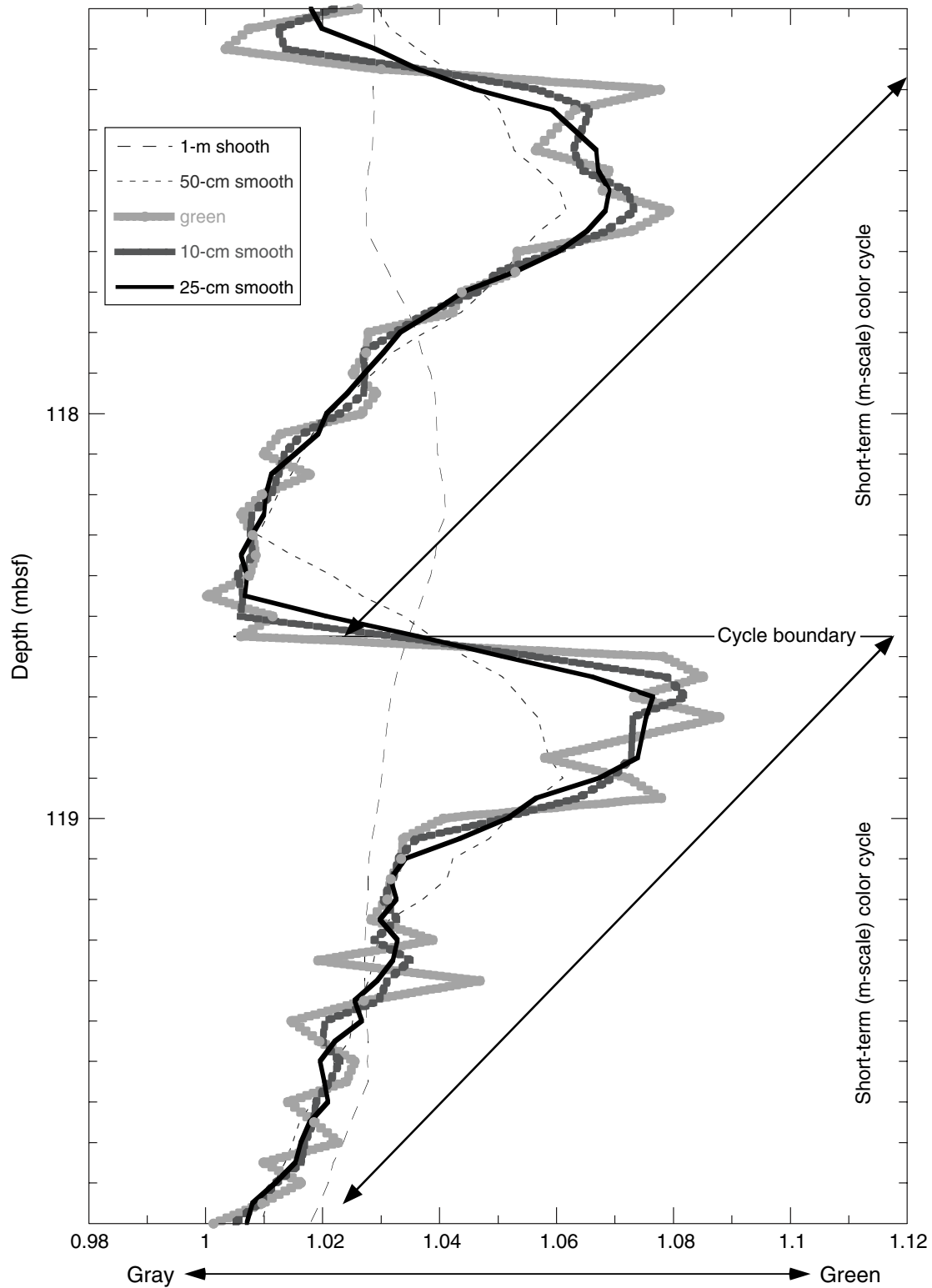


Figure F9. Plot of the comparative test to calibrate the length of the window of the moving average to produce a large-scale curve for the normalization of the 25-cm averaged "green parameter." Two curves obtained with 25- and 50-m windows, respectively, are compared against the 25-cm averaged curve for the whole length of the data set. The 25-m averaged curve is the one that appears to work best to show some decameter-scale trends that will be discussed in this paper, whereas the 50-m smoothed curve is too leveled and excessively diverges from the 25-cm curve. The boundaries of the lithostratigraphic units and those between the sections recovered with different coring devices are also shown. H = hydraulic piston core, X = extended core barrel, R = rotary core barrel.

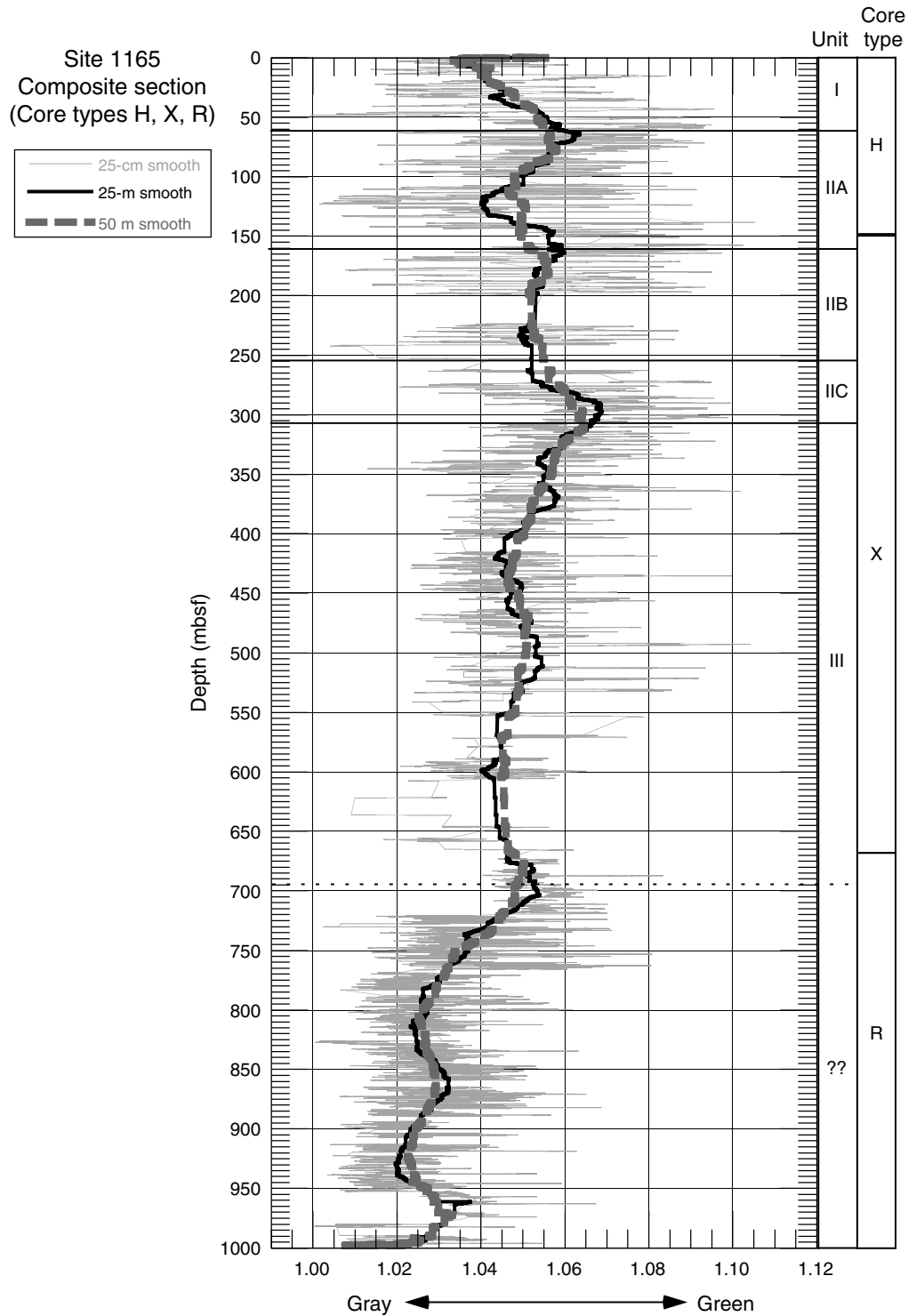
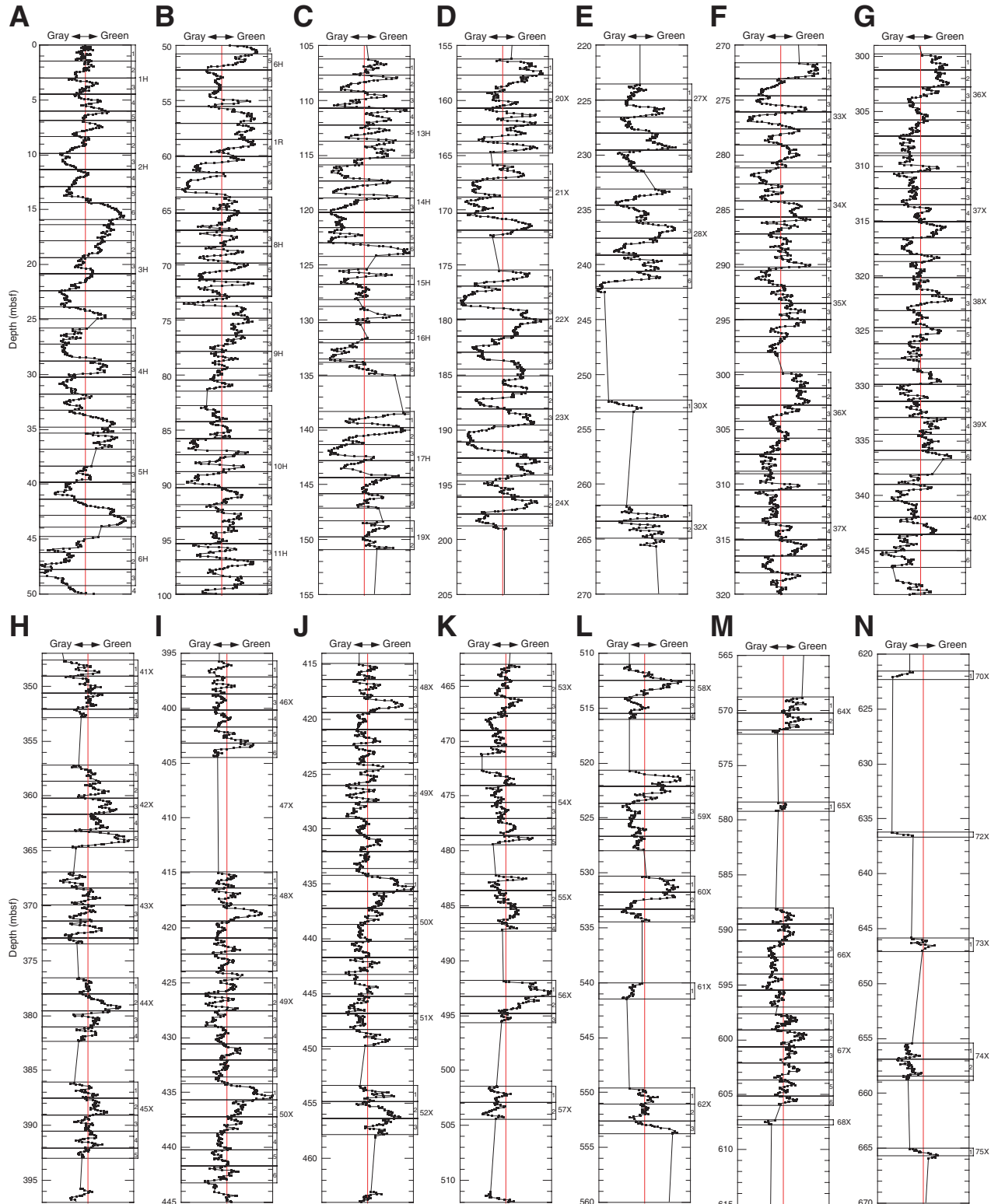
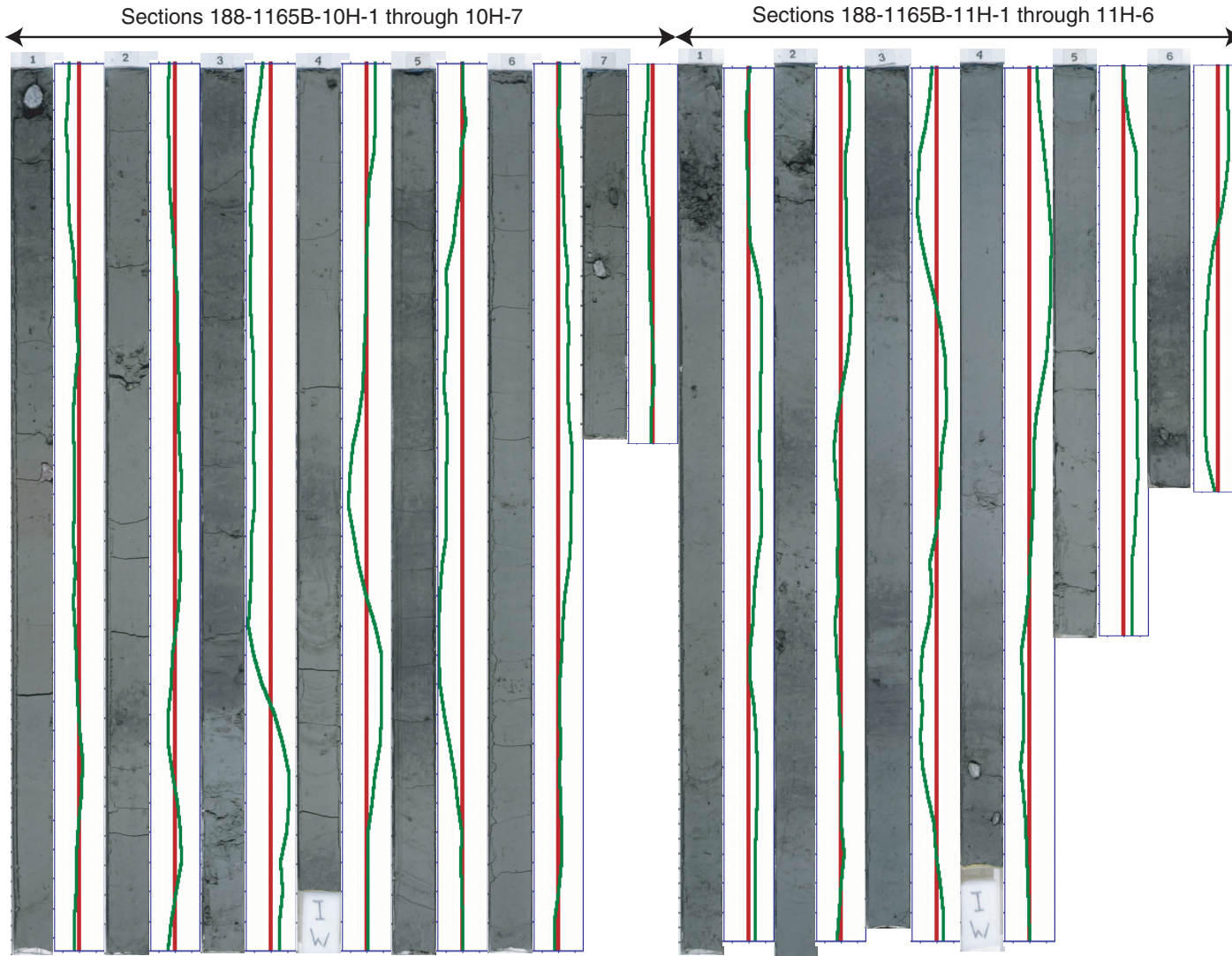


Figure F10. A–N. Plots of 50-m-long segments of the normalized “green parameter” down to 670 mbsf. Samples with negative values correspond to gray facies, whereas positive values correspond to green facies. A vertical line is shown in correspondence of the zero value as reference. For each plot, depth is shown on the left, whereas core and section breaks are indicated (except the not discernible thin seventh sections eventually present) on the right.



**Figure F11.** Composite diagram showing the match between the sections of Cores 188-1165B-10H and 11H with the normalized curve of the 25-cm averaged “green parameter.” The match between the color alternations in the core photos and the proposed curve is adequate, hence providing a link between descriptive (visible) features and numerical series suitable for spectral analyses. The significance of the “green parameter” for the 0- to 670-mbsf column was validated section by section against the core photos, onboard-compiled visual core description sheets, and graphic logs.



**Table T1.** List of the removed samples. (See table note. Continued on next page.)

Core, section, interval (cm)	Motivation	Core, section, interval (cm)	Motivation
188-1165B-1H-1, 124	Stone	36X-0, 15	Overlaps Section 188-1165B-37X-1, 35 cm
1H-4, 130	Stone	36X-0, 20	Overlaps Section 188-1165B-37X-1, 40 cm
1H-1, 126	Hole	36X-0, 25	Overlaps Section 188-1165B-37X-1, 45 cm
1H-1, 128	Hole	36X-1, 5	Stone
3H-1, 70	Stone/fracture	37X-0, 25	Overlaps Section 188-1165B-38X-1, 10 cm
3H-2, 50	Fracture	37X-0, 30	Overlaps Section 188-1165B-38X-1, 15 cm
188-1165C-1R-3, 10	Stone	37X-1, 5	Overlaps Section 188-1165B-36X-1, 35 cm
1R-6, 25	Mud clast	37X-1, 10	Overlaps Section 188-1165B-36X-1, 40 cm
1R-6, 30	Mud clast	37X-1, 15	Overlaps Section 188-1165B-36X-1, 45 cm
188-1165B-8H-3, 149.3	Edge	38X-4, 5	Fracture
8H-3, 40	Stone	38X-5, 150	Edge
8H-7	Edge	40X-1,	Edge
9H-1, 5	Overlaps Section 188-1165B-8H-7, 55 cm	40X-5, 130	Fracture
10H-1, 5	Stone	40X-6, 5	Fracture
10H-1, 70	Stone/fracture	41X-1, 80	Stone
10H-5, 150	Edge	41X-1, 90	Stone
10H-7, 35	Stone	42X-1, 110	Fracture
11H-1, 5	Overlaps Section 188-1165B-10H-7, 55 cm	42X-1, 120	Stone/fracture
11H-1, 10	Overlaps Section 188-1165B-10H-7, 60 cm	42X-1, 125	Stone/fracture
11H-4, 75	Fracture	42X-1, 130	Stone/fracture
13H-2, 115	Stone	42X-1, 135	Stone/fracture
14H-1, 5	Overlaps Section 188-1165B-13H-7, 55 cm	42X-1, 65	Stone
16H-1, 35	Hole	46X-5, 5	Fracture
16H-1, 40	Hole	46X-5, 10	Fracture
16H-4, 10	Fracture	46X-5, 15	Fracture
19X-0, 5	Stone	46X-5, 20	Fracture
19X-0, 10	Fracture	46X-5, 25	Fracture
19X-2, 55	Fracture	48X-1, 15	Stone
20X-1, 10	Stone	48X-2, 105	Fracture/stone
20X-4, 40	Stone	48X-2, 110	Fracture/stone
21X-1, 30	Stone/fracture	48X-2, 115	Fracture/stone
22X-1, 125	Fracture	50X-1, 65	Stone
24X-0, 35	Fracture	51X-1, 115	Stone
24X-0, 40	Void	51X-1, 95	Stone
24X-0, 45	Void	52X-1, 30	Fracture
24X-1, 5	Fracture	52X-3, 20	Fracture
24X-1, 50	Fracture	52X-4, 5	Fracture/clast
30X-1, 105	Fracture	53X-6	Edge
30X-1, 110	Fracture	54X-2, 110	Fracture
30X-1, 115	Fracture	54X-2, 80	Fracture
30X-1, 80	Stone/fracture	56X-2, 75	Stone
30X-1, 90	Fracture	59X-1, 20	Fracture
30X-1, 95	Fracture	59X-1, 30	Fracture
32X-1, 10	Fracture	62X-1, 125	Fracture
32X-1, 135	Fracture	62X-1, 130	Fracture
32X-1, 20	Fracture	62X-3, 70	Fracture
34X-0, 5	Overlaps Section 188-1165B-35X-1, 20 cm	62X-3, 75	Fracture
34X-0, 10	Overlaps Section 188-1165B-35X-1, 25 cm	62X-3, 85	Fracture
34X-0, 15	Overlaps Section 188-1165B-35X-1, 30 cm	62X-3, 90	Fracture
34X-0, 20	Overlaps Section 188-1165B-35X-1, 35 cm	67X-1, 100	Fracture
34X-0, 25	Overlaps Section 188-1165B-35X-1, 40 cm	68X-1, 45	Fracture
34X-1, 5	Edge	68X-1, 50	Fracture
34X-1, 40	Stone	68X-1, 55	Fracture
34X-1, 65	Stone/fracture	68X-1, 60	Fracture
34X-2, 45	Stone/clast	70X-1, 45	Fracture
34X-3, 115	Stone	73X-1, 100	Fracture
34X-3, 35	Stone	73X-1, 110	Fracture
34X-5, 149.8	Edge	73X-1, 80	Fracture
34X-6, 25	Stone	73X-1, 85	Fracture
34X-6, 55	Stone	76X-0, 5	Overlaps Section 188-1165B-2R-2, 16 cm
35X-1, 5	Overlaps Section 188-1165B-34X-7, 35 cm	76X-0, 10	Overlaps Section 188-1165B-2R-2, 22 cm
35X-1, 10	Overlaps Section 188-1165B-34X-7, 40 cm	76X-0, 15	Overlaps Section 188-1165B-2R-2, 26 cm
35X-5, 35	Fracture	76X-0, 20	Overlaps Section 188-1165B-2R-2, 32 cm
36X-0, 5	Overlaps Section 188-1165B-37X-1, 25 cm	76X-0, 25	Overlaps Section 188-1165B-2R-2, 36 cm
36X-0, 10	Overlaps Section 188-1165B-37X-1, 30 cm	76X-0, 30	Overlaps Section 188-1165B-2R-2, 42 cm
		76X-0, 35	Overlaps Section 188-1165B-2R-2, 46 cm
		188-1165C-2R-1, 6	Fracture and Edge
		2R-2, 2	Edge

**Table T1 (continued).**

Core, section, interval (cm)	Motivation
2R-3, 2	Edge
5R-6	Edge
6R-1, 2	Edge
6R-1, 2	Edge
7R-4, 2	Edge
7R-5, 2	Edge
8R-7, 2	Edge
8R-7, 2	Edge
9R-6, 2	Edge
11R-3, 2	Edge
11R-5, 2	Hole
13R-3	Edge
20R-6, 2	Edge
22R-5, 2	Edge
23R-6, 2	Edge
26R-3	Edge
27R-1, 2	Edge
27R-1, 142	Edge
27R-1, 146	Edge
27R-5, 18	Hole
28R-5, 132	Hole
31R-5, 2	Edge
35R-6	Edge

Note: More attention was paid to the upper part of the section (Hole 1165B) where a better preserved record and a better age control are present.

Table T2. Spectral reflectance data, Core 188-1165B-14H between 117 and 120 mbsf. (See table note. Continued on next three pages.)

Core	Type	Section	Top interval (cm)	Depth (mbsf)	Green	25-cm average	25-m average	Anomaly	L*	a*	b*	Munsell	HVC	400 (nm)	410 (nm)	420 (nm)	430 (nm)	440 (nm)	450 (nm)	460 (nm)	470 (nm)	480 (nm)	490 (nm)	500 (nm)
14	H	1	120	117.00	1.026	1.018	1.041	-0.023	43.36	-0.45	1.72	0.6 GY	4.2/3	12.62	12.55	12.49	12.54	12.60	12.65	12.71	12.82	12.93	13.03	13.11
14	H	1	125	117.05	1.007	1.020	1.041	-0.021	38.03	0.13	1.10	4.1 Y	3.7/2	9.71	9.66	9.61	9.67	9.70	9.70	9.74	9.80	9.84	9.89	9.91
14	H	1	130	117.10	1.003	1.029	1.041	-0.012	34.83	0.19	0.88	2.9 Y	3.4/1	8.13	8.08	8.07	8.13	8.14	8.13	8.15	8.19	8.21	8.23	8.25
14	H	1	135	117.15	1.030	1.036	1.041	-0.004	45.48	-0.69	1.91	2.2 GY	4.4/3	13.72	13.69	13.72	13.82	13.88	13.97	14.09	14.24	14.39	14.52	14.61
14	H	1	140	117.20	1.078	1.046	1.041	0.006	47.76	-2.43	3.17	6.7 GY	4.6/7	14.13	14.22	14.35	14.58	14.75	14.95	15.21	15.54	15.86	16.13	16.35
14	H	1	145	117.25	1.063	1.059	1.041	0.019	51.50	-2.18	2.57	7.4 GY	5.0/6	17.57	17.62	17.68	17.85	17.99	18.17	18.42	18.71	19.00	19.28	19.49
14	H	2	5	117.35	1.056	1.067	1.041	0.026	51.95	-2.02	2.23	7.8 GY	5.0/5	18.08	18.14	18.25	18.46	18.60	18.74	18.97	19.25	19.51	19.74	19.94
14	H	2	10	117.40	1.069	1.067	1.041	0.027	48.30	-2.42	2.28	8.7 GY	4.7/6	15.04	15.11	15.26	15.49	15.63	15.78	15.99	16.26	16.53	16.77	16.95
14	H	2	15	117.45	1.068	1.069	1.040	0.029	52.64	-2.48	2.59	8.2 GY	5.1/6	18.25	18.37	18.51	18.72	18.90	19.11	19.39	19.73	20.04	20.35	20.57
14	H	2	20	117.50	1.079	1.068	1.040	0.028	48.96	-2.73	2.85	8.1 GY	4.7/7	15.14	15.23	15.36	15.62	15.80	15.98	16.25	16.59	16.91	17.19	17.41
14	H	2	25	117.55	1.073	1.065	1.041	0.025	46.66	-2.28	2.70	7.2 GY	4.5/6	13.59	13.67	13.84	14.08	14.23	14.38	14.61	14.89	15.15	15.36	15.56
14	H	2	30	117.60	1.053	1.060	1.041	0.020	50.10	-1.74	2.22	6.9 GY	4.9/5	16.62	16.67	16.77	16.97	17.12	17.24	17.42	17.68	17.92	18.12	18.30
14	H	2	35	117.65	1.053	1.053	1.041	0.013	51.09	-1.76	2.34	6.6 GY	5.0/5	17.36	17.41	17.49	17.69	17.83	17.97	18.18	18.45	18.69	18.93	19.11
14	H	2	40	117.70	1.044	1.044	1.041	0.003	40.80	-1.18	1.68	6.2 GY	4.0/4	10.84	10.79	10.81	10.90	10.96	11.05	11.14	11.26	11.39	11.53	11.63
14	H	2	45	117.75	1.042	1.039	1.041	-0.002	39.94	-0.98	1.96	4.5 GY	3.9/4	10.16	10.14	10.19	10.31	10.37	10.44	10.54	10.68	10.79	10.91	11.02
14	H	2	50	117.80	1.028	1.033	1.041	-0.007	42.88	-0.68	1.33	4.5 GY	4.2/2	12.36	12.32	12.30	12.39	12.44	12.49	12.56	12.66	12.75	12.84	12.91
14	H	2	55	117.85	1.027	1.030	1.040	-0.010	41.13	-0.51	1.65	1.4 GY	4.0/3	11.18	11.11	11.10	11.17	11.23	11.26	11.34	11.45	11.55	11.64	11.71
14	H	2	60	117.90	1.025	1.027	1.040	-0.013	45.95	-0.60	1.47	3.0 GY	4.5/3	14.45	14.36	14.33	14.41	14.45	14.50	14.59	14.72	14.84	14.95	15.01
14	H	2	65	117.95	1.029	1.024	1.040	-0.016	42.09	-0.71	1.48	4.1 GY	4.1/3	11.85	11.75	11.75	11.84	11.86	11.90	11.99	12.10	12.21	12.30	12.38
14	H	2	70	118.00	1.027	1.021	1.040	-0.020	44.59	-0.57	1.68	1.8 GY	4.3/3	13.32	13.25	13.26	13.34	13.39	13.45	13.55	13.70	13.82	13.92	14.00
14	H	2	75	118.05	1.013	1.019	1.040	-0.021	41.09	-0.06	1.28	7.1 Y	4.0/2	11.39	11.32	11.28	11.34	11.39	11.40	11.43	11.52	11.60	11.67	11.71
14	H	2	80	118.10	1.010	1.015	1.040	-0.025	39.62	-0.02	1.04	6.6 Y	3.8/1	10.71	10.61	10.55	10.60	10.60	10.61	10.65	10.71	10.75	10.81	10.84
14	H	2	85	118.15	1.018	1.011	1.040	-0.029	45.46	-0.30	1.35	0.3 GY	4.4/2	14.21	14.07	14.08	14.16	14.19	14.22	14.28	14.40	14.49	14.56	14.62
14	H	2	90	118.20	1.010	1.010	1.040	-0.030	37.70	-0.08	0.79	8.2 Y	3.7/1	9.79	9.64	9.58	9.62	9.63	9.62	9.64	9.70	9.74	9.77	9.80
14	H	2	95	118.25	1.006	1.010	1.041	-0.031	41.24	0.07	0.88	4.5 Y	4.0/1	11.78	11.67	11.61	11.63	11.65	11.66	11.66	11.71	11.77	11.82	11.84
14	H	2	100	118.30	1.008	1.008	1.041	-0.033	41.69	0.02	0.88	5.2 Y	4.0/1	12.11	12.00	11.92	11.92	11.93	11.94	11.95	12.01	12.05	12.09	12.11
14	H	2	105	118.35	1.009	1.006	1.041	-0.035	41.69	0.02	1.05	5.4 Y	4.0/1	11.89	11.80	11.78	11.83	11.85	11.86	11.89	11.96	12.01	12.06	12.09
14	H	2	110	118.40	1.007	1.007	1.041	-0.033	45.11	0.03	0.93	5.0 Y	4.4/1	14.38	14.22	14.14	14.16	14.17	14.19	14.20	14.27	14.34	14.36	14.41
14	H	2	115	118.45	1.000	1.007	1.041	-0.034	37.81	0.26	0.72	0.8 Y	3.7/1	9.97	9.83	9.74	9.74	9.72	9.71	9.72	9.75	9.78	9.83	9.82
14	H	2	120	118.50	1.011	1.021	1.041	-0.020	39.16	-0.08	1.02	7.8 Y	3.8/1	10.42	10.34	10.31	10.34	10.34	10.35	10.39	10.46	10.52	10.56	10.59
14	H	2	125	118.55	1.006	1.036	1.041	-0.004	35.31	0.26	1.37	3.3 Y	3.4/2	8.29	8.17	8.14	8.18	8.19	8.19	8.25	8.32	8.36	8.39	8.42
14	H	2	130	118.60	1.078	1.051	1.041	0.010	46.89	-2.60	2.80	7.8 GY	4.5/7	13.64	13.74	13.90	14.14	14.30	14.48	14.74	15.04	15.35	15.60	15.79
14	H	2	135	118.65	1.085	1.066	1.041	0.025	47.28	-3.01	2.57	9.5 GY	4.6/7	14.12	14.15	14.28	14.52	14.69	14.86	15.10	15.42	15.73	15.98	16.19
14	H	2	140	118.70	1.073	1.077	1.041	0.036	49.22	-2.67	2.36	9.2 GY	4.8/6	15.75	15.78	15.91	16.14	16.29	16.43	16.65	16.96	17.26	17.51	17.71
14	H	2	145	118.75	1.088	1.075	1.041	0.035	49.08	-3.30	2.51	0.2 G	4.8/7	15.35	15.48	15.61	15.85	16.04	16.23	16.49	16.82	17.16	17.45	17.68
14	H	3	5	118.85	1.058	1.074	1.041	0.033	48.15	-1.90	2.23	7.3 GY	4.7/5	15.13	15.14	15.23	15.46	15.60	15.72	15.89	16.14	16.39	16.58	16.73
14	H	3	10	118.90	1.072	1.067	1.041	0.027	43.61	-2.27	2.40	7.7 GY	4.2/6	11.69	11.79	11.96	12.19	12.34	12.46	12.64	12.87	13.10	13.31	13.46
14	H	3	15	118.95	1.078	1.057	1.041	0.016	48.16	-2.69	2.66	8.4 GY	4.7/7	14.69	14.78	14.93	15.14	15.31	15.49	15.72	16.01	16.32	16.61	16.81
14	H	3	20	119.00	1.041	1.052	1.040	0.011	48.17	-1.15	2.07	5.2 GY	4.7/4	15.41	15.39	15.46	15.63	15.73	15.83	16.00	16.20	16.38	16.54	16.67
14	H	3	25	119.05	1.034	1.044	1.041	0.003	46.31	-0.90	1.73	4.8 GY	4.5/3	14.31	14.31	14.35	14.48	14.57	14.65	14.76	14.91	15.04	15.17	15.28
14	H	3	30	119.10	1.033	1.034	1.041	-0.006	47.09	-0.80	1.98	2.9 GY	4.6/3	14.67	14.72	14.75	14.88	15.00	15.10	15.22	15.38	15.56	15.71	15.79
14	H	3	35	119.15	1.032	1.032	1.040	-0.009	40.84	-0.60	1.94	1.5 GY	4.0/3	10.73	10.68	10.73	10.85	10.92	10.97	11.07	11.22	11.33	11.42	11.50
14	H	3	40	119.20	1.031	1.033	1.041	-0.008	42.32	-0.58	1.91	1.3 GY	4.1/3	11.58	11.59	11.66	11.78	11.83	11.89	11.99	12.12	12.24	12.34	12.41
14	H	3	45	119.25	1.028	1.030	1.041	-0.011	44.56	-0.56	1.81	1.4 GY	4.3/3	13.18	13.15	13.15	13.26	13.33	13.40	13.50	13.62	13.73	13.85	13.93
14	H	3	50	119.30	1.039	1.033	1.041	-0.008	41.08	-0.71	2.22	1.5 GY	4.0/4	10.63	10.63	10.71	10.87	10.96	11.02	11.12	11.25	11.37	11.50	11.60
14	H	3	55	119.35	1.019	1.032	1.041	-0.009	43.05	-0.39	1.13	1.8 GY	4.2/2	12.76	12.67	12.59	12.62	12.65	12.68	12.74	12.83	12.91	12.98	13.02
14	H	3	60	119.40	1.047	1.029	1.041	-0.011	45.67	-1.07	2.71	2.7 GY	4.4/5	13.27	13.28	13.35	13.50	13.63	13.76	13.90	14.10	14.29	14.46	14.61
14	H	3	65	119.45	1.027	1.026	1.041	-0.015	43.05	-0.46	1.86	0.5 GY	4.2/3	12.16	12.14	12.18	12.27	12.30	12.38	12.49	12.60	12.71	12.83	12.90

Table T2 (continued).

Core	Type	Section	Top interval (cm)	Depth (mbsf)	510 (nm)	520 (nm)	530 (nm)	540 (nm)	550 (nm)	560 (nm)	570 (nm)	580 (nm)	590 (nm)	600 (nm)	610 (nm)	620 (nm)	630 (nm)	640 (nm)	650 (nm)	660 (nm)	670 (nm)	680 (nm)	690 (nm)	700 (nm)
14	H	1	120	117.00	13.21	13.30	13.37	13.39	13.48	13.54	13.58	13.55	13.50	13.50	13.47	13.38	13.33	13.24	13.16	13.05	12.92	12.77	12.63	12.50
14	H	1	125	117.05	9.95	9.99	10.04	10.04	10.10	10.14	10.18	10.21	10.19	10.21	10.23	10.22	10.23	10.21	10.22	10.19	10.15	10.13	10.10	10.05
14	H	1	130	117.10	8.27	8.32	8.37	8.36	8.40	8.45	8.48	8.49	8.44	8.48	8.53	8.51	8.51	8.52	8.54	8.54	8.53	8.52	8.52	8.50
14	H	1	135	117.15	14.72	14.82	14.90	14.94	15.00	15.03	15.05	15.06	14.99	14.97	14.91	14.81	14.71	14.62	14.56	14.44	14.32	14.23	14.10	13.96
14	H	1	140	117.20	16.57	16.72	16.86	16.88	16.99	17.01	16.96	16.87	16.67	16.49	16.22	15.97	15.72	15.37	15.03	14.74	14.43	14.08	13.77	13.46
14	H	1	145	117.25	19.70	19.83	19.97	20.02	20.09	20.11	20.04	19.93	19.72	19.53	19.32	19.03	18.74	18.43	18.13	17.81	17.45	17.09	16.78	16.48
14	H	2	5	117.35	20.13	20.26	20.36	20.42	20.47	20.47	20.39	20.28	20.09	19.92	19.72	19.45	19.20	18.92	18.65	18.36	18.05	17.71	17.40	17.16
14	H	2	10	117.40	17.12	17.24	17.34	17.35	17.41	17.40	17.31	17.19	17.00	16.79	16.53	16.28	16.06	15.74	15.46	15.16	14.83	14.50	14.23	13.95
14	H	2	15	117.45	20.78	20.93	21.05	21.10	21.16	21.15	21.07	20.93	20.71	20.48	20.19	19.87	19.58	19.22	18.86	18.52	18.15	17.75	17.43	17.13
14	H	2	20	117.50	17.65	17.77	17.90	17.96	18.00	17.99	17.88	17.78	17.55	17.32	17.04	16.75	16.45	16.08	15.77	15.42	15.06	14.72	14.37	14.00
14	H	2	25	117.55	15.77	15.88	16.00	16.06	16.08	16.11	16.09	15.97	15.80	15.60	15.40	15.15	14.93	14.62	14.31	14.04	13.73	13.42	13.16	12.89
14	H	2	30	117.60	18.48	18.57	18.67	18.73	18.80	18.81	18.76	18.71	18.56	18.40	18.18	18.01	17.79	17.51	17.31	17.05	16.74	16.45	16.21	15.98
14	H	2	35	117.65	19.29	19.42	19.52	19.59	19.67	19.67	19.62	19.54	19.40	19.25	19.05	18.81	18.64	18.38	18.13	17.86	17.56	17.26	17.02	16.77
14	H	2	40	117.70	11.72	11.77	11.81	11.84	11.91	11.90	11.88	11.86	11.77	11.71	11.61	11.52	11.44	11.27	11.11	10.98	10.83	10.65	10.49	10.35
14	H	2	45	117.75	11.11	11.17	11.29	11.31	11.33	11.34	11.37	11.36	11.28	11.25	11.17	11.08	10.99	10.85	10.77	10.63	10.45	10.31	10.20	10.04
14	H	2	50	117.80	12.99	13.05	13.12	13.15	13.16	13.18	13.20	13.21	13.13	13.11	13.04	12.97	12.90	12.78	12.68	12.59	12.47	12.33	12.21	12.10
14	H	2	55	117.85	11.80	11.83	11.93	11.98	12.03	12.05	12.09	12.11	12.02	12.00	11.96	11.92	11.89	11.79	11.69	11.60	11.50	11.39	11.26	11.11
14	H	2	60	117.90	15.08	15.19	15.25	15.27	15.34	15.37	15.36	15.38	15.33	15.27	15.20	15.16	15.07	15.00	14.87	14.76	14.67	14.54	14.39	14.27
14	H	2	65	117.95	12.45	12.51	12.59	12.61	12.67	12.69	12.69	12.65	12.61	12.58	12.53	12.45	12.38	12.28	12.19	12.07	11.96	11.86	11.74	11.63
14	H	2	70	118.00	14.10	14.17	14.27	14.27	14.33	14.36	14.39	14.40	14.35	14.32	14.28	14.19	14.13	14.06	14.00	13.87	13.71	13.60	13.53	13.39
14	H	2	75	118.05	11.76	11.80	11.85	11.88	11.94	11.99	12.02	12.05	12.01	12.04	12.01	12.00	12.02	12.01	11.93	11.92	11.86	11.79	11.73	11.67
14	H	2	80	118.10	10.89	10.93	10.97	11.00	11.02	11.08	11.11	11.12	11.07	11.11	11.10	11.12	11.12	11.07	11.01	11.00	10.99	10.92	10.86	10.81
14	H	2	85	118.15	14.69	14.75	14.84	14.88	14.94	14.97	15.01	15.02	14.94	14.93	14.93	14.89	14.85	14.78	14.73	14.65	14.54	14.47	14.40	14.29
14	H	2	90	118.20	9.84	9.84	9.89	9.89	9.94	9.95	10.01	10.01	9.95	9.95	9.97	9.95	9.94	9.93	9.90	9.85	9.79	9.74	9.74	9.72
14	H	2	95	118.25	11.88	11.91	11.93	11.98	12.04	12.05	12.04	12.12	12.09	12.09	12.12	12.10	12.13	12.12	12.08	12.09	12.03	11.98	11.94	11.90
14	H	2	100	118.30	12.14	12.20	12.25	12.24	12.34	12.37	12.36	12.39	12.39	12.42	12.39	12.37	12.36	12.31	12.31	12.27	12.22	12.16	12.07	12.01
14	H	2	105	118.35	12.14	12.20	12.24	12.25	12.29	12.35	12.39	12.41	12.37	12.40	12.40	12.39	12.39	12.37	12.35	12.32	12.27	12.26	12.24	12.16
14	H	2	110	118.40	14.48	14.49	14.53	14.57	14.66	14.69	14.70	14.73	14.70	14.71	14.74	14.71	14.72	14.66	14.65	14.63	14.55	14.51	14.47	14.39
14	H	2	115	118.45	9.84	9.89	9.89	9.91	9.97	10.02	10.03	10.04	10.04	10.08	10.09	10.13	10.12	10.08	10.11	10.11	10.09	10.08	10.06	10.03
14	H	2	120	118.50	10.64	10.66	10.72	10.70	10.79	10.80	10.82	10.85	10.81	10.84	10.85	10.80	10.79	10.76	10.72	10.68	10.62	10.59	10.57	10.48
14	H	2	125	118.55	8.49	8.52	8.56	8.61	8.63	8.67	8.73	8.76	8.76	8.78	8.79	8.83	8.85	8.81	8.82	8.83	8.80	8.78	8.78	8.76
14	H	2	130	118.60	15.98	16.12	16.25	16.28	16.33	16.29	16.23	16.13	15.91	15.72	15.47	15.22	14.97	14.65	14.37	14.05	13.71	13.41	13.11	12.83
14	H	2	135	118.65	16.41	16.53	16.62	16.66	16.70	16.66	16.54	16.40	16.14	15.91	15.63	15.32	15.02	14.68	14.32	13.98	13.61	13.25	12.93	12.60
14	H	2	140	118.70	17.90	18.02	18.14	18.20	18.22	18.16	18.06	17.97	17.70	17.44	17.22	16.95	16.64	16.28	15.99	15.66	15.30	14.93	14.62	14.35
14	H	2	145	118.75	17.90	18.04	18.14	18.15	18.20	18.13	18.00	17.82	17.52	17.24	16.93	16.57	16.20	15.82	15.45	15.06	14.67	14.28	13.88	13.55
14	H	3	5	118.85	16.90	17.01	17.10	17.18	17.22	17.23	17.16	17.13	16.93	16.79	16.58	16.35	16.19	15.91	15.66	15.42	15.15	14.87	14.62	14.39
14	H	3	10	118.90	13.59	13.72	13.81	13.84	13.88	13.87	13.80	13.72	13.56	13.42	13.23	12.99	12.76	12.53	12.32	12.08	11.80	11.55	11.34	11.10
14	H	3	15	118.95	17.00	17.15	17.30	17.29	17.32	17.32	17.24	17.11	16.89	16.68	16.40	16.11	15.85	15.50	15.18	14.85	14.50	14.17	13.84	13.52
14	H	3	20	119.00	16.80	16.91	17.01	17.06	17.12	17.16	17.17	17.11	17.02	16.92	16.81	16.67	16.56	16.39	16.23	16.05	15.85	15.64	15.47	15.29
14	H	3	25	119.05	15.40	15.46	15.53	15.60	15.65	15.67	15.67	15.67	15.57	15.51	15.44	15.32	15.22	15.09	14.98	14.86	14.69	14.52	14.38	14.22
14	H	3	30	119.10	15.92	16.02	16.07	16.15	16.24	16.26	16.26	16.26	16.22	16.17	16.06	15.96	15.89	15.75	15.63	15.49	15.33	15.19	15.03	14.85
14	H	3	35	119.15	11.59	11.69	11.77	11.79	11.84	11.88	11.93	11.93	11.84	11.83	11.78	11.74	11.71	11.60	11.52	11.42	11.30	11.20	11.10	10.96
14	H	3	40	119.20	12.51	12.60	12.71	12.74	12.80	12.86	12.87	12.86	12.80	12.77	12.76	12.69	12.62	12.51	12.45	12.33	12.18	12.06	11.95	11.81
14	H	3	45	119.25	14.03	14.12	14.22	14.28	14.33	14.36	14.38	14.40	14.35	14.31	14.26	14.21	14.13	14.02	13.93	13.81	13.70	13.60	13.46	13.29
14	H	3	50	119.30	11.70	11.79	11.90	11.94	12.03	12.08	12.11	12.09	12.03	11.99	11.95	11.87	11.78	11.67	11.57	11.43	11.29	11.16	11.02	10.86
14	H	3	55	119.35	13.08	13.13	13.17	13.21	13.27	13.29	13.28	13.32	13.25	13.26	13.21	13.16	13.11	13.02	12.97	12.89	12.77	12.66	12.56	12.46
14	H	3	60	119.40	14.77	14.93	15.06	15.11	15.23	15.27	15.27	15.25	15.17	15.15	15.02	14.88	14.76	14.57	14.42	14.24	14.03	13.82	13.62	13.42
14	H	3	65	119.45	12.99	13.07	13.15	13.19	13.29	13.32	13.34	13.37	13.31	13.29	13.26	13.20	13.15	13.04	12.99	12.89	12.75	12.65	12.55	12.43

Table T2 (continued).

Core	Type	Section	Top interval (cm)	Depth (mbsf)	Green	25-cm average	25-m average	Anomaly	L*	a*	b*	Munsell	HVC	400 (nm)	410 (nm)	420 (nm)	430 (nm)	440 (nm)	450 (nm)	460 (nm)	470 (nm)	480 (nm)	490 (nm)	500 (nm)
14	H	3	70	119.50	1.015	1.027	1.041	-0.014	40.06	-0.13	1.14	8.4 Y	3.9/.2	10.82	10.75	10.73	10.79	10.81	10.82	10.87	10.96	11.02	11.07	11.13
14	H	3	75	119.55	1.019	1.022	1.041	-0.019	44.86	-0.40	1.28	1.5 GY	4.4/.2	13.75	13.65	13.64	13.75	13.79	13.81	13.90	14.02	14.13	14.20	14.25
14	H	3	80	119.60	1.026	1.020	1.041	-0.021	41.41	-0.54	1.46	2.1 GY	4.0/.2	11.38	11.33	11.34	11.41	11.45	11.51	11.60	11.69	11.78	11.88	11.95
14	H	3	85	119.65	1.024	1.020	1.041	-0.021	44.30	-0.62	1.17	5.0 GY	4.3/.2	13.42	13.38	13.34	13.41	13.46	13.50	13.55	13.65	13.76	13.85	13.88
14	H	3	90	119.70	1.014	1.021	1.041	-0.020	36.41	-0.11	0.95	8.4 Y	3.5/.1	8.68	8.67	8.74	8.85	8.90	8.91	8.94	8.98	9.01	9.05	9.08
14	H	3	95	119.75	1.019	1.018	1.041	-0.023	37.19	-0.13	1.41	8.2 Y	3.6/.2	8.80	8.85	8.95	9.06	9.13	9.17	9.20	9.27	9.35	9.39	9.42
14	H	3	100	119.80	1.023	1.016	1.041	-0.025	39.07	-0.48	1.12	3.2 GY	3.8/.2	10.13	10.09	10.12	10.21	10.25	10.27	10.31	10.40	10.46	10.52	10.57
14	H	3	105	119.85	1.010	1.015	1.041	-0.026	40.32	-0.12	0.70	9.5 Y	3.9/.1	11.23	11.12	11.10	11.14	11.16	11.17	11.19	11.23	11.26	11.31	11.33
14	H	3	110	119.90	1.016	1.012	1.041	-0.029	45.62	-0.24	1.24	9.7 Y	4.4/.2	14.37	14.30	14.28	14.34	14.35	14.38	14.45	14.55	14.63	14.71	14.76
14	H	3	115	119.95	1.010	1.008	1.041	-0.033	38.39	0.06	1.24	5.1 Y	3.7/.2	9.84	9.75	9.75	9.82	9.84	9.84	9.90	9.97	10.00	10.04	10.09
14	H	3	120	120.00	1.001	1.007	1.041	-0.034	39.41	0.14	0.44	0.9 Y	3.8/.1	10.88	10.78	10.71	10.74	10.74	10.72	10.73	10.76	10.77	10.78	10.79

Note: Only a portion of this table appears here. The complete table is available in [ASCII](#).

Table T2 (continued).

Core	Type	Section	Top interval (cm)	Depth (mbsf)	510 (nm)	520 (nm)	530 (nm)	540 (nm)	550 (nm)	560 (nm)	570 (nm)	580 (nm)	590 (nm)	600 (nm)	610 (nm)	620 (nm)	630 (nm)	640 (nm)	650 (nm)	660 (nm)	670 (nm)	680 (nm)	690 (nm)	700 (nm)
14	H	3	70	119.50	11.17	11.19	11.25	11.27	11.28	11.31	11.39	11.42	11.36	11.35	11.37	11.36	11.32	11.27	11.23	11.18	11.12	11.04	10.97	10.90
14	H	3	75	119.55	14.31	14.35	14.43	14.47	14.49	14.52	14.57	14.57	14.50	14.48	14.46	14.41	14.40	14.34	14.24	14.15	14.07	13.98	13.88	13.76
14	H	3	80	119.60	12.03	12.06	12.14	12.16	12.21	12.22	12.22	12.23	12.18	12.18	12.14	12.07	12.04	11.95	11.89	11.79	11.68	11.61	11.49	11.36
14	H	3	85	119.65	13.95	14.02	14.07	14.10	14.17	14.16	14.14	14.16	14.11	14.05	13.99	13.93	13.86	13.76	13.70	13.60	13.45	13.33	13.23	13.12
14	H	3	90	119.70	9.12	9.16	9.18	9.20	9.26	9.26	9.29	9.31	9.28	9.28	9.27	9.26	9.25	9.18	9.19	9.17	9.10	9.05	9.04	9.01
14	H	3	95	119.75	9.49	9.52	9.58	9.62	9.69	9.73	9.71	9.74	9.74	9.73	9.73	9.70	9.69	9.66	9.62	9.59	9.53	9.47	9.43	9.36
14	H	3	100	119.80	10.62	10.65	10.72	10.74	10.78	10.78	10.79	10.77	10.73	10.75	10.69	10.64	10.62	10.54	10.47	10.41	10.32	10.23	10.15	10.06
14	H	3	105	119.85	11.34	11.38	11.43	11.45	11.48	11.50	11.52	11.50	11.46	11.50	11.50	11.47	11.45	11.40	11.38	11.35	11.30	11.24	11.16	11.10
14	H	3	110	119.90	14.83	14.87	14.94	15.00	15.06	15.05	15.08	15.13	15.08	15.07	15.07	15.02	15.00	14.91	14.86	14.78	14.66	14.55	14.46	14.38
14	H	3	115	119.95	10.15	10.18	10.24	10.27	10.33	10.34	10.40	10.43	10.37	10.43	10.44	10.42	10.40	10.38	10.39	10.38	10.35	10.32	10.29	10.27
14	H	3	120	120.00	10.83	10.84	10.86	10.85	10.88	10.87	10.95	10.98	10.94	10.96	10.98	10.96	10.97	10.97	10.95	10.95	10.93	10.92	10.91	10.88